A national laboratory of the U.S. Department of Energy
Office of Energy Efficiency & Renewable Energy

National Renewable Energy Laboratory

Innovation for Our Energy Future

FY 2005 Midyear Progress Report on Solar Radiometry and Metrology Task PVC57301

October 1, 2004 to March 15, 2005

D.R. Myers, T.L. Stoffel, A.A. Andreas, S.M. Wilcox,
I. Reda, M. Anderberg, P. Gotseff, and B. Kay

Technical Report
NREL/TP-560-37954
September 2005

NREL is operated by Midwest Research Institute • Battelle Contract No. DE-AC36-99-GO10337

FY 2005 Midyear Progress Report on Solar Radiometry and Metrology Task PVC57301

October 1, 2004 to March 15, 2005

D.R. Myers, T.L. Stoffel, A.A. Andreas, S.M. Wilcox, I. Reda, M. Anderberg, P. Gotseff, and B. Kay

Prepared under Task No. PVC57301

Technical Report
NREL/TP-560-37954
September 2005

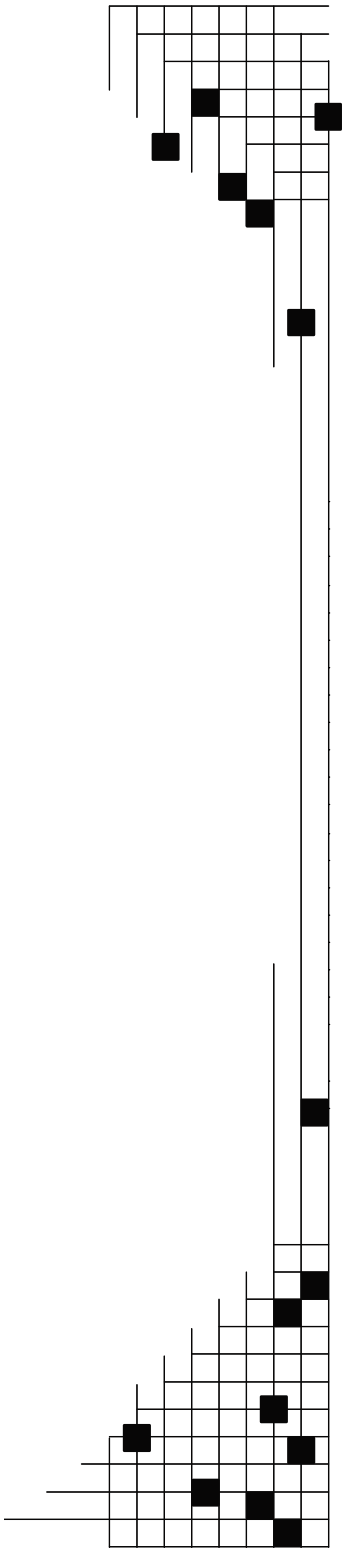

National Renewable Energy Laboratory
1617 Cole Boulevard, Golden, Colorado 80401-3393
303-275-3000 • www.nrel.gov

Operated for the U.S. Department of Energy
Office of Energy Efficiency and Renewable Energy
by Midwest Research Institute • Battelle

Contract No. DE-AC36-99-GO10337

Preface

This report documents technical details for work performed in the Solar Radiometry and Metrology Task PVC57301 in the period from October 1 2004 to March 15 2005. The Task has conducted improved broadband and spectral calibrations, measurements, and modeling activities supporting NREL's Photovoltaic Systems Engineering Project, and Photovoltaic Measurements and Characterization Projects. The task calibrated nine spectroradiometer systems used to classify and characterize continuous and pulsed solar simulators for NREL and PV industry partners. These instruments were used to acquire and use data to correct for deviations from standard reporting condition reference spectra. Tests were conducted to evaluate the suitability of replacing an obsolescent group of spectroradiometers with new diode array and scanning spectrometers. We conducted detailed studies thermal offsets, a significant source of measurement error in broadband radiometers measuring total hemispherical solar radiation, and published peer reviewed papers describing the research and correction schemes. An intercomparison of absolute cavity radiometers was conducted to assure the stable maintenance of the World Radiometric Reference at NREL. Preparations are underway for travel to the World Radiation Data Center, Davos, Switzerland, to accomplish the transfer of the World Radiometric Reference to NREL reference absolute cavity radiometers, in compliance with International Standards Organization ISO standard 17025 requirements for traceability of NREL's solar measurements. A new, more accurate data acquisition system was purchased to upgrade broadband radiometer calibrations, and is undergoing testing and development of software to integrate with existing Radiometer Characterization and Calibrations software. Improvements have been made to the Solar Radiation Research Laboratory web-accessible data ensemble, permitting hourly summary data to be generated from any data collection station accessible through the site. We have documented over 135 technical exchanges with photovoltaic industry, academic, other national laboratories, and individuals.

Contents

List of Figures

List of Tables

1.0 Introduction

The Solar Radiometry and Metrology Task is a component of the Photovoltaic Systems Engineering Project at the National Renewable Energy Laboratory (NREL). The task provides traceable optical radiometric calibrations and measurements to photovoltaic (PV) researchers and the PV industry. Table 1.1 shows the task description prepared for fiscal year 2005 Solar Program Annual operating Plan.

Table 1.1 Fiscal Year 2005 Annual operating plan task description

Task Title	Org'n	Task Description	FY 2005 Budget ($K)
Solar Radiometry & Metrology	NREL	This task provides world-class and traceable solar radiometric measurements, instrumentation, and metrology required by the PV Systems Engineering Project and other projects.	625

A collection of nine spectroradiometer systems are periodically calibrated against National Institute of Standards and Technology sources, and are used to perform measurements of natural sunlight and solar simulators. These measurements are integral to the ISO 17025 accreditation of NREL Secondary Solar Reference Cell Calibrations. The spectral distributions of continuous and pulsed solar simulators are measured to characterize simulator performance and data for computing PV performance with respect to standard reporting conditions. Spectroradiometer systems are also constantly evaluated to identify areas of improvement, or the ability to upgrade to more appropriate systems as technology advances.

Traceability of NREL broadband solar radiometer calibrations to the World Radiometric Reference (WRR) is accomplished through periodic (every five year) participation in World Meteorological Organization (WMO) International Pyrheliometer Comparisons (IPC) conducted at the WMO World Radiation Center at Davos, Switzerland. Quality assurance of the WRR at NREL is accomplished during annual NREL Pyrheliometer Comparisons. A collection of four NREL absolute cavity radiometers maintain the WRR at NREL, and are the reference for the calibration of about 300 broadband radiometers by the task per year.

The task calibrates nine to ten spectral and more than 180 broadband radiometers every year. We characterized pyranometer thermal offset errors with laboratory and spectral modeling tools; developed a simple scheme to correct pyranometer data for known responsivity variations; and measured detailed spectral distributions of the NREL and industry solar simulators. Optical metrology functions have been integrated into the NREL quality system and audited for ISO 17025 compliance.

1.1 Background and Objectives

The major activity and thrust of this project is the near-term and long-term performance monitoring, characterization, and modeling of emerging-technology, small (< 5 kWp),

grid-connected, prototype systems installed and operating at NREL's Outdoor Test Facility (OTF). Critical to this effort is a supporting task that provides world-class and traceable measurements and instrumentation for solar radiometry. The resultant precision and accuracy of the PV system (and module) performance measurements is determined by the quality, precision, and accuracy of the measurements of the incident (on the PV arrays) solar irradiance (i.e. "power in"). We support the development of industry-consensus/adopted codes, standards, addressing radiometric components in testing PV devices and systems. This project is integral to the Solar Energy Technologies Program Multi-year Technical Plan, providing credible/independent data, analyses, and assessments of the performance and reliability metrics that are required in benchmarking the candidate technologies and supporting the systems-driven-approach to R&D management. The next section summarizes the task deliverables described in the FY 2005 AOP for this task.

1.2 Major FY 2005 Milestones and Deliverables

The major expected FY 2005 accomplishments of the task include:

- Continued world-class solar radiometric, and therefore PV system performance, measurements and instrumentation
- Reporting research progress in technical reports and journal articles

Table 1.2 summarizes the deliverables described in the FY 2005 AOP. This rest of this report describes key research and measurement accomplishments in the first six months of fiscal year 2005 activities supporting the above deliverables

Table 1.2. FY 2005 Task PVC57301 Milestones and Deliverables

Milestone or Deliverable	Task No.	Due Date	Priority Level	Status
Complete mid-year and annual summary report of NIST traceable/ISO 17025 compliant optical calibrations of NREL and PV industry radiometers.	2	03/31/05 09/30/05	4	This Report
Complete proposed revised ASTM pyranometer calibration standards, reflecting state-of-the-art capabilities.	2	03/31/05	5	Accomplished 1/15/05 See section 3.2.8
Complete technical & logistical preparations for WMO International Pyrheliometer Comparison, Davos, Switzerland, October, 2005.	2	08/31/05	5	In progress See section 3.1
Select spectroradiometer and verify integration in PV Reference Cell calibration procedures.	2	08/31/05	4	In progress see section 2.5

2. 0 Spectroradiometric Calibrations and Measurements

Spectral distribution of the optical radiation encountered during testing of PV devices either in the laboratory or outdoors is needed to properly correct test data to standard reporting conditions [1] , or assess observed variation in long term PV array and system performance. The Solar Radiometry and Metrology task manages a collection of spectroradiometer systems appropriate to assist NREL researchers and PV industry partners identify spectral issues with performance data. A subset of these instruments is used in calibrating secondary PV reference cells. This NREL activity was accredited in accordance with ISO 17025 requirements at the end of 2004. One part of the ISO accreditation is the requirement for traceability of all calibrations and measurements to the International System (SI) of units. Table 2.1 lists the spectroradiometer systems, useful wavelength range, and main applications. Figure 1.1 shows large and small-scale solar simulators used for PV performance testing in the laboratory.

Table 2.1. NREL Spectrometer Systems

Spectroradiometer System	Wavelength Range	Application
OL-750 #1	280 nm -1800 nm	X-25 simulator spectral tuning and monitoring
OL-750 #2	280 nm -1800 nm	Large Area continuous Solar Simulator (LACCS) Integrated Pulse measurements (Spire 240) check
OL-754	250 nm - 800 nm	Reference for UV and Photometer Radiometer Calibration UV source characterization; UV hazard identification
LI-1800 PRS 102	300 nm -1100nm	PV reference cell calibration outdoors; X-25, Large Area Continuous; Laboratory small scale simulators, special outdoor measurements.
LI-1800 PRS 158	300 nm -1100nm	
LI-1800 PRS 174	300 nm -1100nm	
Li-1800 PRS 218	300 nm -1100 nm	
Analytical Spectral Devices ASD FieldSpec	350 nm -2100 nm	Natural and Artificial Source Characterization; integrated Pulse simulator measurement checks
Pulse Analysis Spectroradiometer System	250 nm -1800 nm	Detailed Characterization Pulse lamp sources; Spire 240, High Intensity Pulse Solar Simulator (HIPSS)

In each instance, a measure of the quantity and quality of optical radiation seen by the PV devices is important in establishing technology performance. For laboratory sources, it is important that the quality of the illumination, as measured by the spectral distribution of the source, is comparable to sunlight, or characterized for the departure from the spectral distribution of sunlight.

Fig. 2.1. Large (left) and small (right) scale solar simulators for evaluating PV performance in the laboratory.

2.1 Spectroradiometer Calibrations

Fig 2.2 Scanning grating monochromator with integrating sphere input optic.

Spectroradiometers used at the National Renewable Energy Laboratory (NREL) include classic scanning grating monochromators and diode array spectroradiometers. Figure 2.2 is an example of a scanning grating monochromator system being set up to measure an illumination source in an environmental chamber. The calibration of these spectroradiometers is performed with respect to standards of spectral irradiance purchased directly form the National Institute of Standards and Technology (NIST) Optical Technology Division[†]. NIST provides a calibrated 1000 W incandescent tungsten halogen lamp with tabulated spectral irradiance data at about 30 wavelengths [2] . The lamp is calibrated at a certain direct current (DC), usually 8.2 amperes, and a specified distance (500 mm) from the front surface of the lamp bi-post pins. The user must reproduce the current specified by NIST, with stability better than 0.01%. The calibration geometry, especially the calibration distance, must also be reproduced as accurately as possible. This requires stable DC power supplies and precision calibration geometry set-up fixtures. Figure 2.3 is an example of the calibration geometry for a diode array spectrometer, showing the lamp, NIST spectral irradiance data (inset), and a close-up of the spectral irradiance standard lamp. NIST supplies a statement of uncertainty with the spectral calibration, as shown in table 2.2. A typical spectral calibration consists of

[†] see http://physics.nist.gov/Divisions/Div844/facilities/fascal/fascal.html

recording the response of the spectroradiometer system, including input optics, monochromator, and detectors, when viewing the calibration source (spectral standard lamp) at each wavelength. Figure 2.4 displays a typical response curve and the spectral distribution of the lamp source.

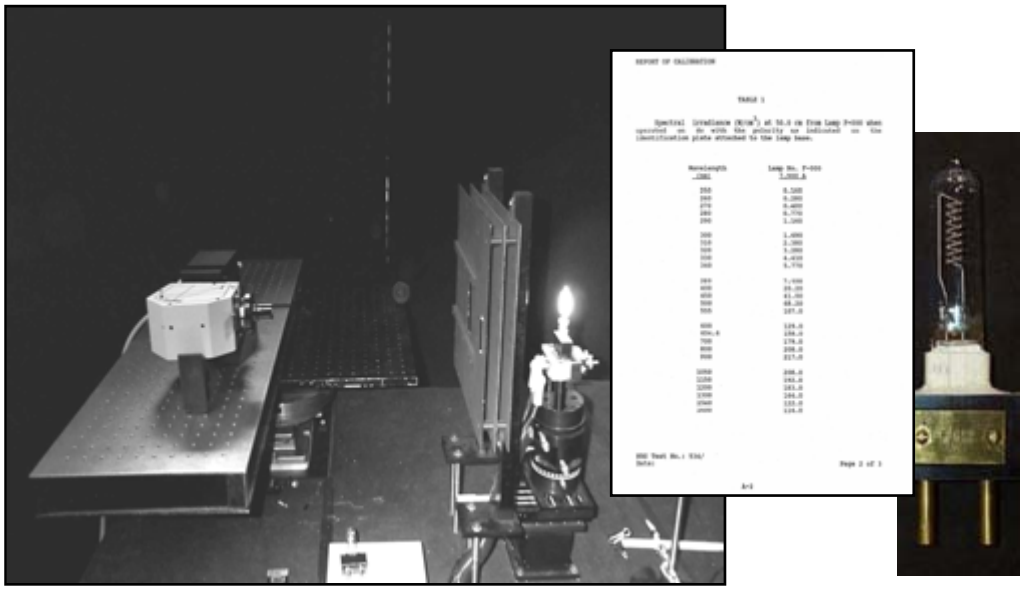

Fig.2.3. Example of spectral irradiance calibration configuration using NIST Standard of Spectral Irradiance (at right).

Table 2.2. NIST specified uncertainty in standards of spectral irradiance.

Wavelength (nm)	Typical Values (W/cm^{-3})	Relative Expanded Uncertainty , k=2 (%)
250	0.2	1.8
350	7.0	1.1
655	170	0.9
900	215	1.1
1600	115	1.4
2400	40	4.4

In addition to the NIST calibration uncertainty mentioned above, additional sources of uncertainty in the local laboratory calibrations, and in various measurement scenarios must be accounted for, as described in the next section.

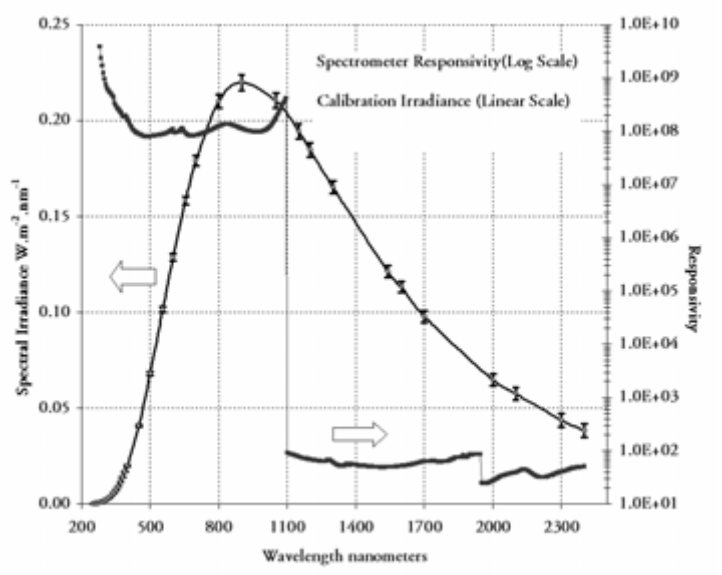

Fig. 2.4. NIST standard lamp spectral irradiance (filled circles with NIST error bars; (linear axis) and typical spectrometer response function (log axis, step at 1100 nm and 1950 nm due to detector change).

During the first quarter of FY 05, we calibrated all nine spectroradiometer systems listed in Table 3. Calibration results, reports, and data are recorded in an electronic data base (Atmospheric Radiation Measurement (ARM) program Instrument Management system, or AIM) accessible at http://www.nrel.gov/aim/database.html.

Each calibration consists of a wavelength check by measuring emission sources of known wavelength, as shown in Figure 2.5

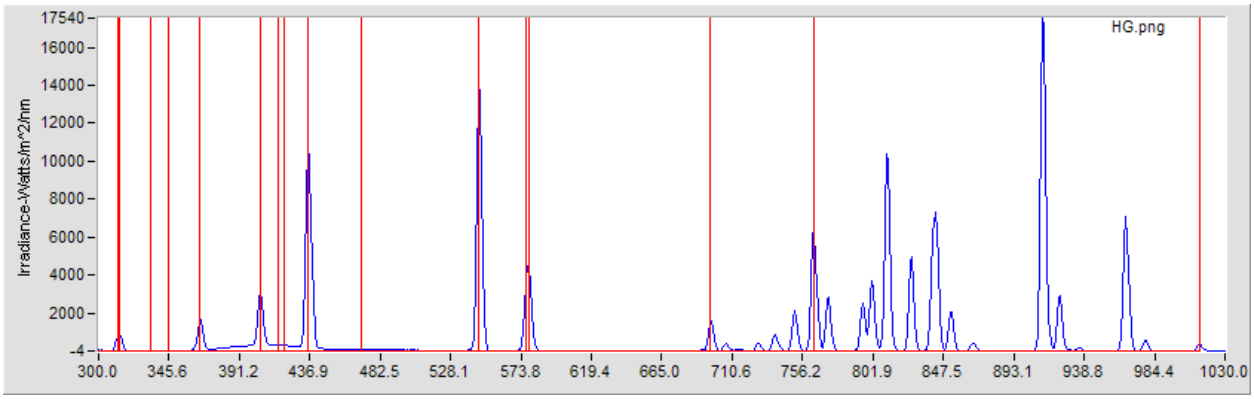

Fig. 2.5. Wavelength test scan (peaks) of known emission wavelengths (vertical lines) to establish spectroradiometer wavelength accuracy.

After taking corrective action regarding wavelength test results that are out of tolerance, the spectroradiometer responsivity is generated using a NIST lamp. The same lamp is then measured as an unknown, to assure the calibration response was properly generated. Figure 2.6 is plot of such the ratio of a check measurement to the NIST lamp data.

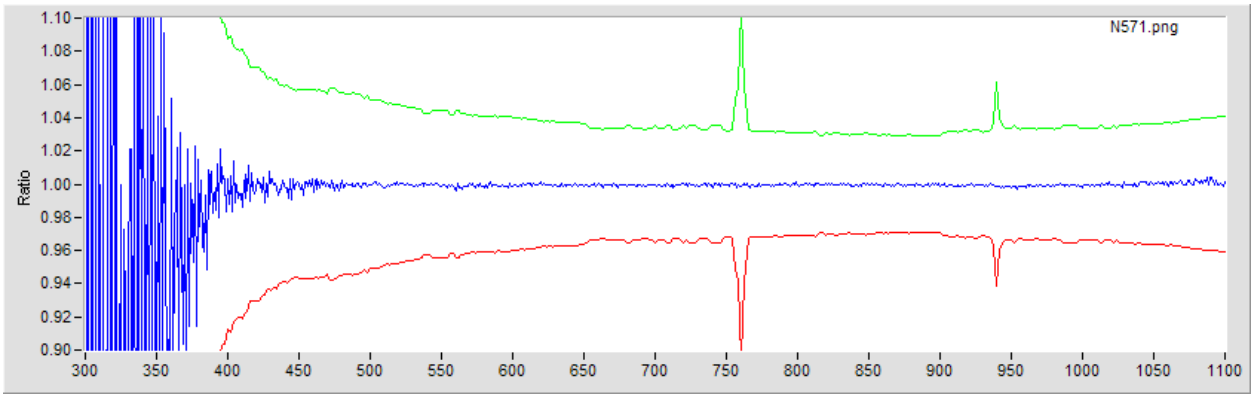

Fig. 2.6. Ratio of check measurement to NIST lamp data after spectral calibration (center line). Top and bottom lines are uncertainty limits for the measurement. Noise at short wavelengths (left) is due to poor signal-to-noise ratio for this unit.

Finally, the new calibration is compared with the last calibration to provide information on radiometer drift with time. Figure 6 shows the ratio of a new to old calibration.

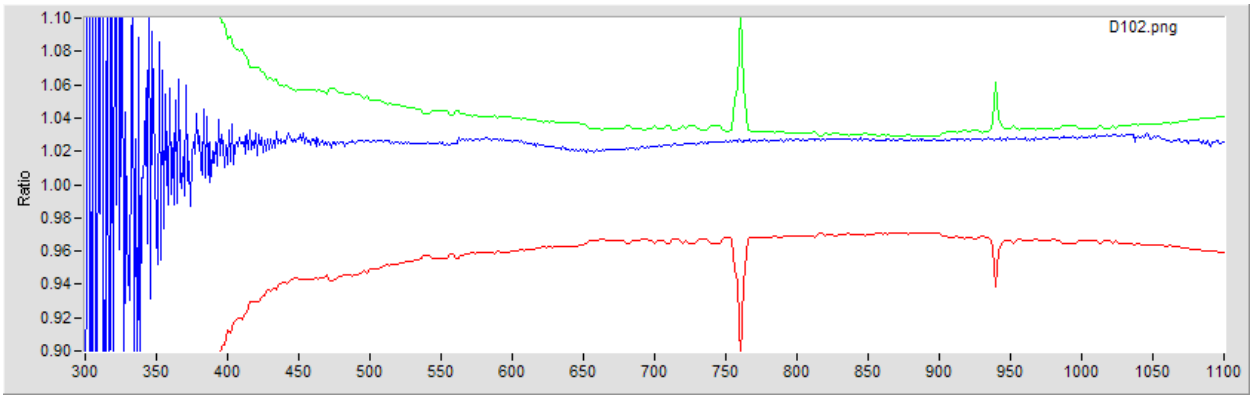

Fig. 2.7. Ratio (center line) of new to previous calibration showing changes in responsivity of the test spectrometer. Top and bottom envelopes are uncertainty limits for measured data.

The final new calibration file and a narrative calibration report are entered into the AIM data base. The report is used to elucidate any special problems or issues with the spectroradiometer system. Figure 2.8 is an example AIM data base record for one of the Li-1800 Licor spectroradiometers used to monitor the Spectrolab X-25 solar simulator, the Large Area Continuous Solar Simulator, or outdoor data during PV reference cell calibrations.

All NREL spectrometers are calibrated at nearly the same time (within 1 week of each other) to prevent the possibility of differing times between calibrations becoming an issue when the same source is measured by several spectrometers with disparate results.

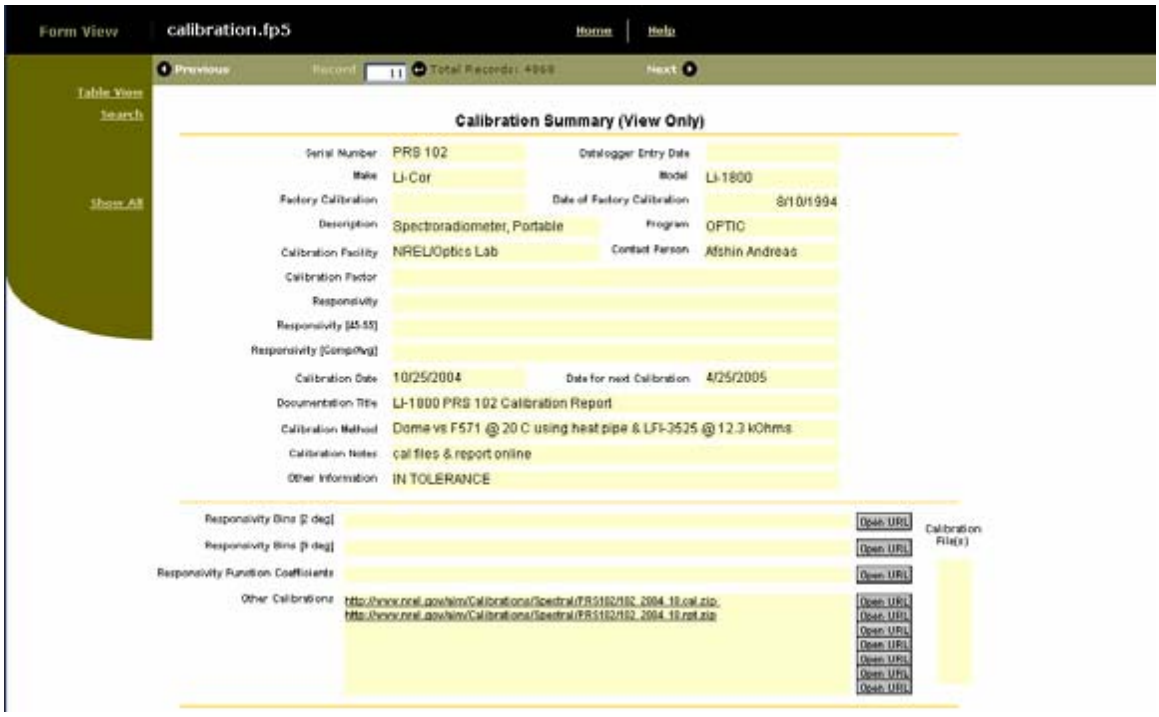

Fig. 2.8. AIM database entry for spectroradiometer calibrations. ASCII versions of calibration files and report documents are accessed though links at the bottom of the frame.

Besides posting calibration results in the AIM database, new calibration files and reports are posted on a secure internal NREL server for use by the PV Measurements Group for easy access to historical data and reports, in case questions arise during new measurement activities. Calibration intervals have been set at six-month intervals because changes such those shown in Figure 2.7 can be seen over this interval. Longer intervals between calibrations can result in greater drift and the need for larger corrections. In addition, we performed research that shows that calibration files are sensitive to atmospheric water vapor (relative humidity, RH) in the laboratory, and we scheduled calibrations at times (spring, fall) when the relative humidity in the NREL Optical Metrology Laboratory is consistent with the expected RH in measurement laboratories at NREL.

2.2 Spectral Calibration Uncertainty Analysis

In the first quarter of FY 05, we revisited our calibration and measurement uncertainty analysis for the Optronic Laboratory OL-750 and OL-754 spectrometer systems, which are critical reference spectrometers.

Each measurement only approximates the quantity being measured, and is incomplete without a quantitative uncertainty. Every element of a measurement system contributes elements of uncertainty. Historically, uncertainty analysis treated sources of uncertainty in terms of "random" and "bias" types. Random sources of uncertainty were related to the standard deviation or variance of measured data sets. Biases were estimates of deviations from a "true value". Total uncertainty U was computed from: $U^2 = \Sigma\ (\text{Bias})^2 + \Sigma(2*\text{Random})^2$. The factor of 2 in the random term was necessary to "inflate" the random component to provide approximately a 95% confidence interval for the computed U.

The Guide to Measurement Uncertainty (GUM) of the International Bureau of Weights and Measures is presently the accepted guide for measurement uncertainty [3]. The GUM defines Type A uncertainty values as derived from statistical methods, and Type B sources as evaluated by "other means", such as scientific judgment, experience, specifications, comparisons, or calibration data. The GUM defines the concept of a "standard uncertainty" for each uncertainty type, which is an estimate of an "equivalent" standard deviation (of a specified distribution). The GUM replaces the historical factor of two with a "coverage factor", *k* (dependent upon the known or assumed statistical distribution of uncertainties), and $U^2 = \Sigma\ (\text{Type B})^2 + \Sigma\ (k*\ \text{Type A})^2$. For small (n<20) samples from a normal distribution, *k* may be selected from the student's t-distribution[4]. U is the "Expanded Uncertainty", and *k* is usually in the range of 2 to 3, for confidence intervals of 95% and 99%, respectively. When a result, R, is functionally dependent upon several i=1,...,n variables, x_i, the familiar propagation of error formula $U^2 = \sum_i (\partial_{Xi} R \cdot\ e_{Xi})^2$ is used. U is the uncertainty in the resultant, e_{xi} is the estimated uncertainty in variable x_i, and $\partial_{xi}R$ is the partial derivative of the response R with respect to variable x_i, called the sensitivity function for variable x_i.

2.3 Laboratory Spectral Calibration Uncertainty

Using the NIST calibration lamp in the laboratory, the specifications of the power supply, geometric alignment, and accuracy of the current supplied to the lamp must be considered. For each a Type A and Type B estimate of uncertainty is based on specifications, previous measurements, or educated estimates. The specifications of the spectroradiometer, such as wavelength accuracy and precision, detector noise equivalent power, stray light levels, temperature coefficients, and so on, must also be considered. Table 2.3 lists the uncertainties associated with operating equipment and alignment of a spectroradiometer in the laboratory for the spectral range 250 nm to 1600 nm. An analysis similar to that in Table 2.3 can be conducted on a wavelength-by-wavelength basis. "Combined" uncertainties are the root-sum-square (RSS) of the Type A and Type B standard uncertainties; "expanded" uncertainty is the RSS of type A and Type B standard uncertainties with the coverage factor *k* applied to achieve the desired confidence interval. An asterisk indicates that an entry is a standard uncertainty (equivalent standard deviation).

Table 2.3. Uncertainties for 95% confidence interval, spectroradiometer calibration

TYPE A (Statistical)	UNC (%)	STD UNC (%)
Distance (2/500 mm)	0.80	0.400
Wavelength Precision	0.01	0.005
Power current (Irr dI/di %)	*0.20	0.200
NIST Lamp Precision	1.13	0.565
Detector Sig/Noise	1.0e-4	5.0e-5
Sig Detection Sys	1.00	0.500
Temp sensitivity	1.00	0.500
Observed Noise (% reading)	3.00	1.500

TYPE B	UNC (%)	STD UNC (%)
NIST Transfer	1.82	0.910
Distance	0.8	0.400
Stray Light	1e-4	0.00005
Lamp Alignment	0.10	0.050
Power Current	*0.20	0.200
Shunt Bias	0.04	0.020
Wavelength	0.01	0.005

TOTAL	UNCERT (%)	STD UNCERT (%)
Type A	3.600	1.808
Type B	2.001	1.015
COMBINED	**4.154**	**2.077**

EFFECTIVE DEG. OF FREEDOM	>100
COVERAGE FACTOR (k)	2
CONFIDENCE INTERVAL	95%
EXPANDED UNCERTAINTY	**4.147%**

The test of the quality of an uncertainty analysis is that no measured values fall outside the expected range of uncertainty. By repeated measurements of several spectral irradiance standard lamps using a spectroradiometer system calibrated using a single lamp, we can evaluate the analysis in Table 5. Figure 2.9 compares the measurement of seven NIST spectral irradiance standards as unknown sources, using a system calibrated using an eighth lamp. The wavelength-by-wavelength envelope for the standard uncertainties is shown, showing that the estimates in Table 5 are conservative, except for the region below 400 nm, where the sensitivity and signal-to-noise ratio of the detectors decreases greatly. Lamp 403, which had been extensively used to test purposes after the

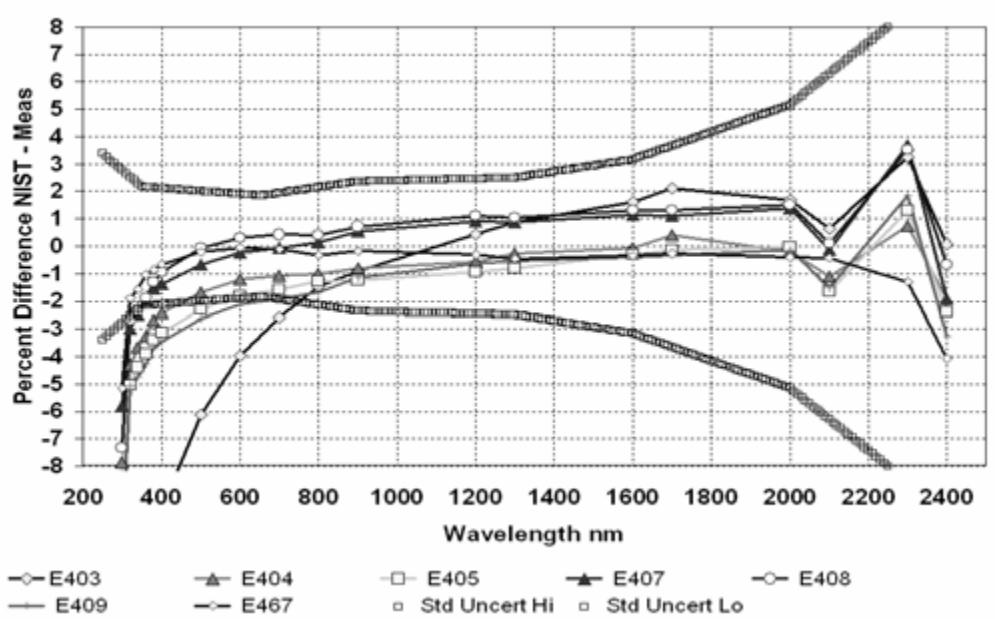

Fig. 2.9. Percent differences between NIST and Measured spectral irradiance at NIST data wavelengths for seven NIST spectral irradiance standard lamps (symbols on lines) measured with a spectrometer system calibrated using an eighth lamp. The envelope of estimated *standard uncertainties* is shown by the thick-hatched lines. Lamp 403 (diamond) had over 100 hours of use above the NIST specified useful lifetime of 50 operational hours.

50 hours of specified useful life, shows serious degradation in the ultraviolet-visible part of the spectrum. The other lamps had less than 10 hours of use.

The data in Figure 2.9 was collected under conditions identical to calibration conditions in the metrology laboratory. When measurements are conducted under different conditions, and of significantly different spectral distributions, there will be changes in the uncertainty envelope related to differences between the calibration spectral distribution and the distribution being measured (the effect of slit scattering function), stability of the spectroradiometer system, differing environmental conditions, etc. which need to be evaluated and combined with the calibration uncertainty on a case by case basis.

2.4 Example Spectral Measurement Results

Utilizing the systems described above, several measurements of note were accomplished in the first half of FY 2005. Measurement of the NREL Large Area Continuous Solar simulator (pictured at left in Figure 1.1), have shown that the simulator has degraded somewhat from a Class A classification (according to American Society for Testing and Materials, or ASTM, Standard E-927 on the Classification of Solar Simulators [5]) to Class B. The progress of the change is documented in the series of measurement shown in Figure 2.10. Figure 2.11 shows the latest classification analysis.

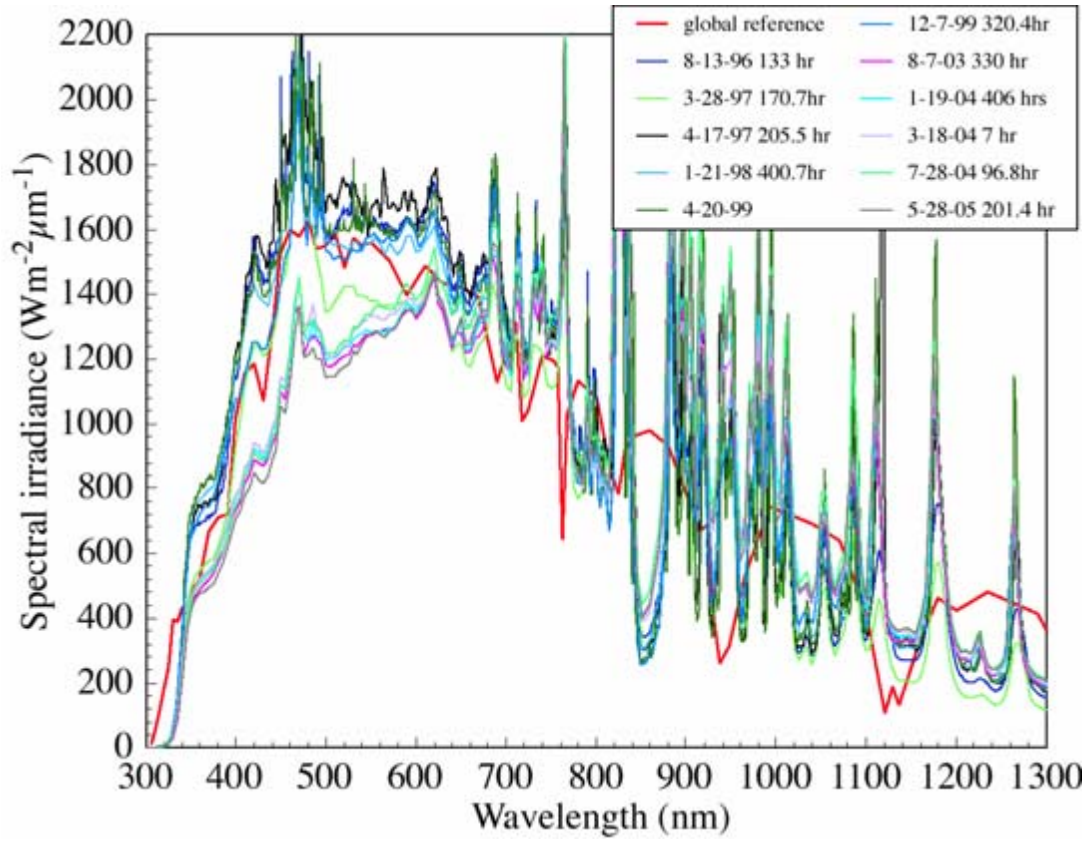

Fig. 2.10. Series of NREL LACSS spectral distribution measurements showing degradation from ASTM Class A to ASTM Class B with respect to the global reference spectrum.

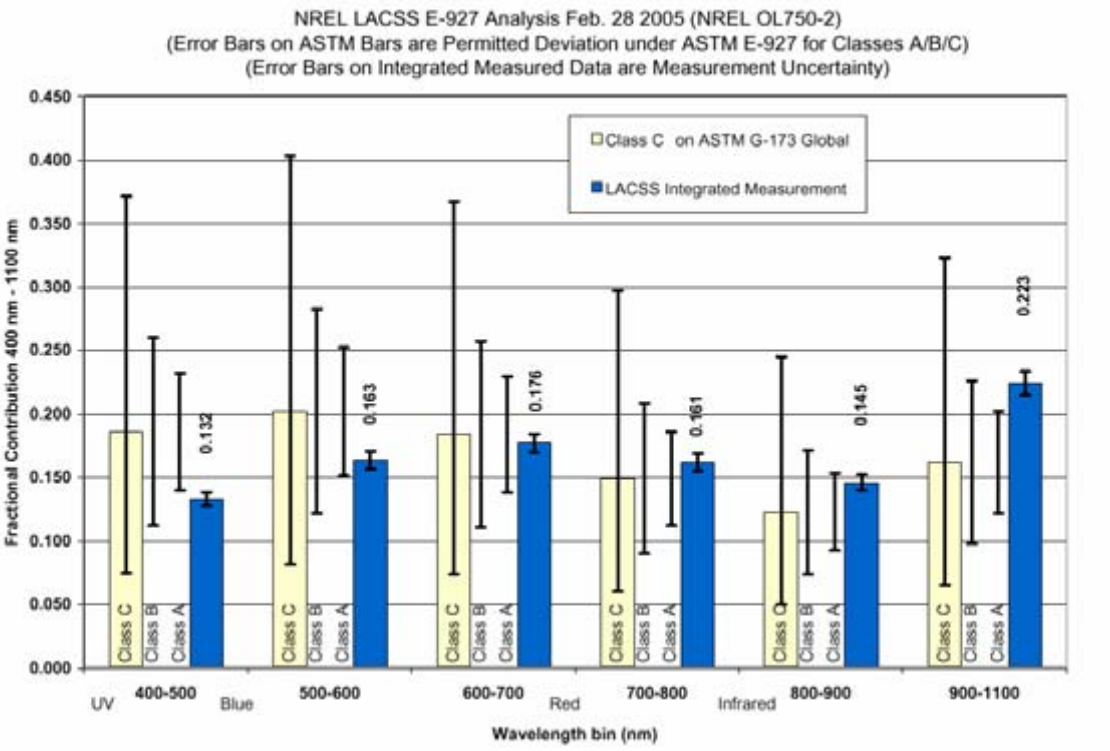

Fig 2.11. ASTM E-927 Classification analysis of LACSS spectral bands. Note low values of LACSS spectra in blue band (400 nm-500 nm) and excess Infrared (900 nm-1100 nm band). Measured data are solid bars on far right, with measurement uncertainty limits. Error bars to left are allowable limits for each classification within band.

An example of our support of PV industry was a request by Shell Solar at Camarillo, CA to have the spectral distributions of two different pulse solar simulators. Shell noticed that the same modules measured on the two different simulators were given significantly different ratings. They suspected spectral distribution differences were the cause of the differences. The NREL Pulse Analysis Spectroradiometer System (PASS) is capable of measuring the spectral content of any part of a flash lamp pulse of light. Shell contacted NREL and asked for our assistance in quantifying the differences between the simulators.

From February 6 to February 9, 2005, we measured the spectral distributions of the Shell Solar Spire Model 460i simulator, and their Large Area Pulse Solar Simulator (LAPSS) using the NREL PASS. Figure 2.12 shows the pulse profiles in time, with the portion of the pulse selected for the spectral measurements denoted by the heavy portion of the curve.

Figure 2.13 shows the measured spectral distribution compared with the reference spectral distribution for the Spire 460 simulator. Figures 2.14 and 2.15 show the ASTM E-927 classification analysis for both simulators in a format identical to that in Figure 2.11. These analyses show the Shell Solar Spire 460 to meet Class B specifications, and the LAPSS simulator to meet Class C specifications.

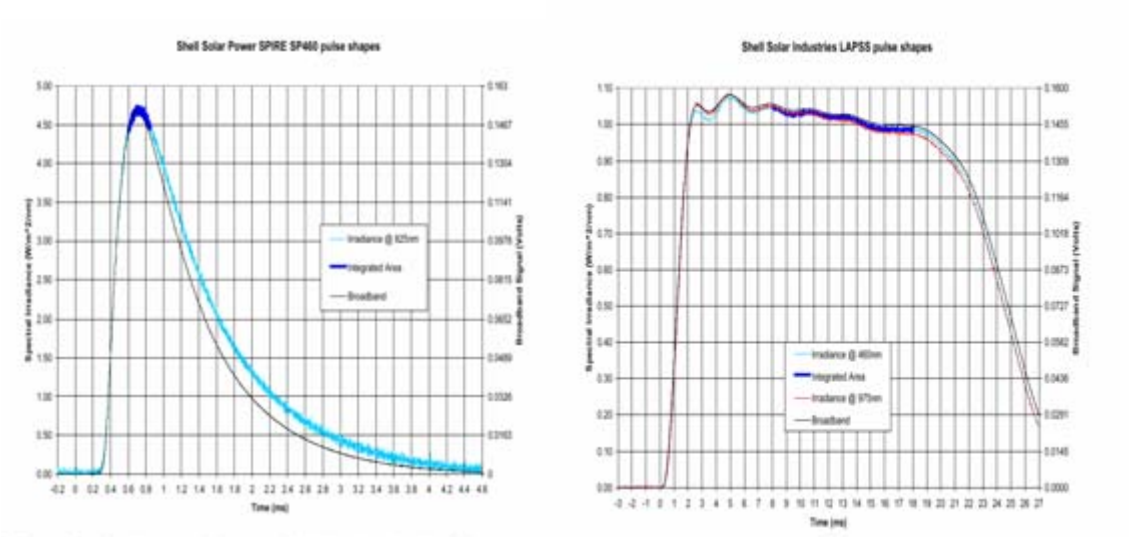

Fig. 2.12 Light pulse shapes for Shell Solar Spire 460 solar simulator (left, 0 ms to 3 ms) and LAPSS (right, 0 ms to 27 ms

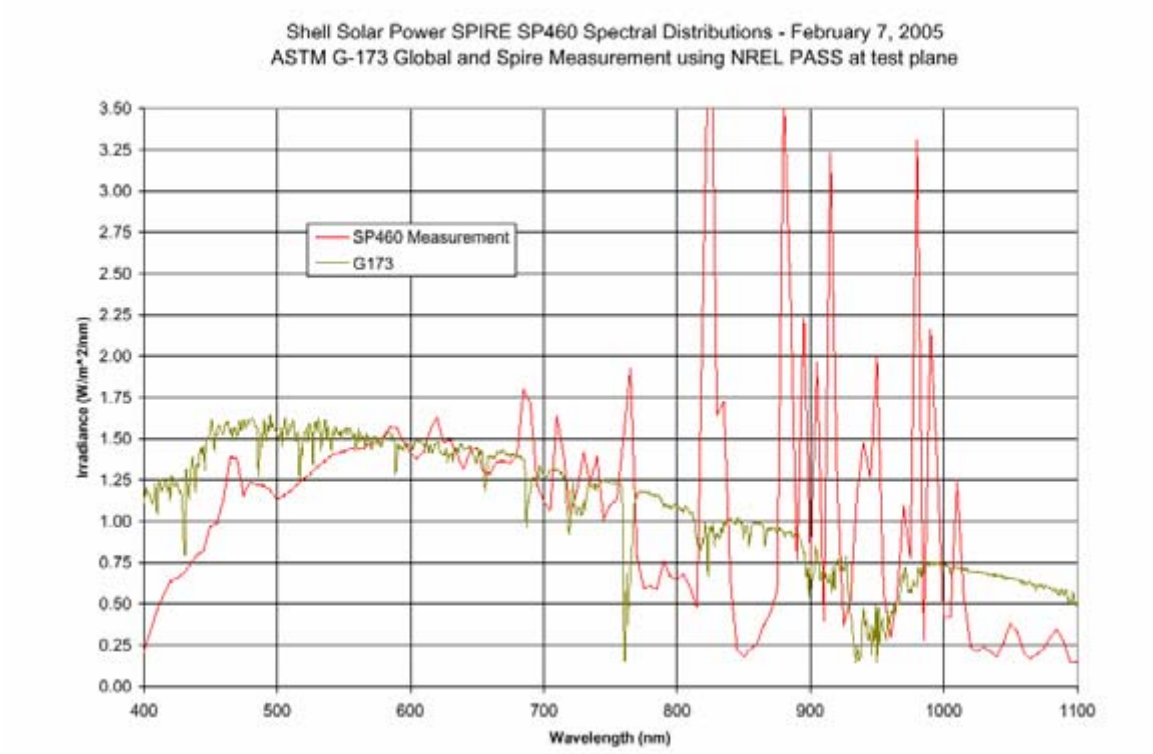

Fig. 2.13. NREL PASS Measured spectral distribution of Shell Solar Spire 460 simulator (lower line) and reference global solar spectrum (upper line).

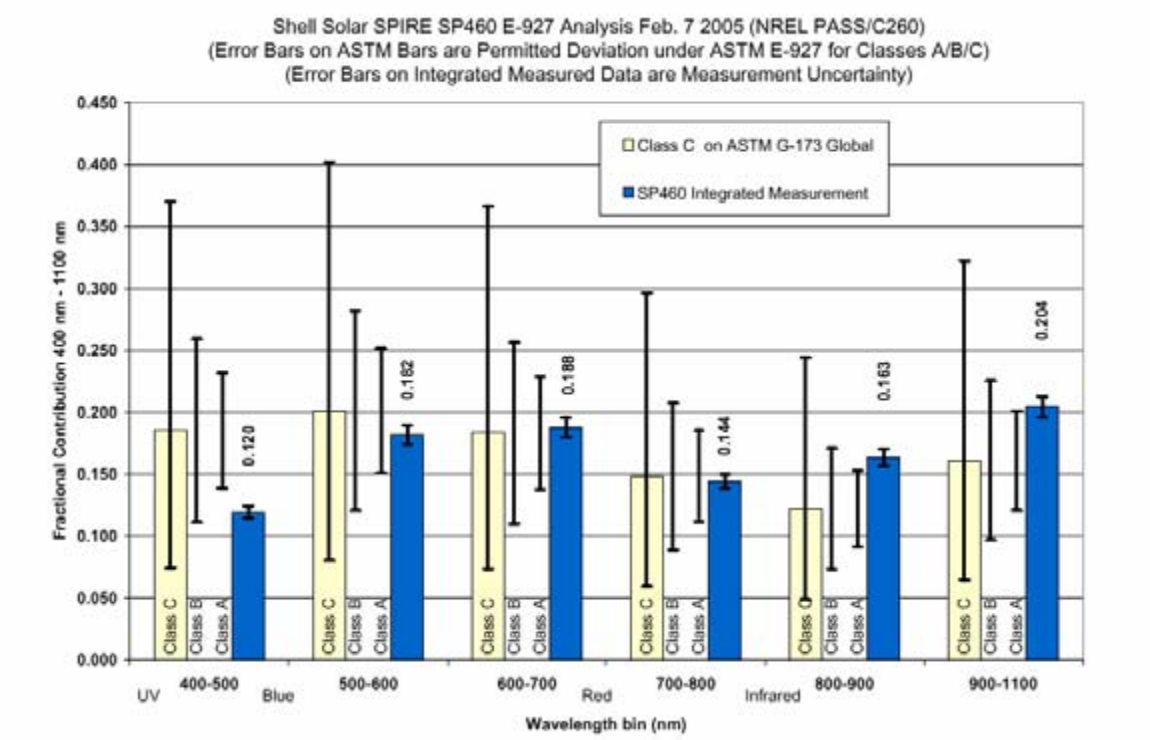

Fig 2.14. ASTM E-927 Classification of Shell Solar Spire 460 simulator based upon NREL PASS Spectral data.

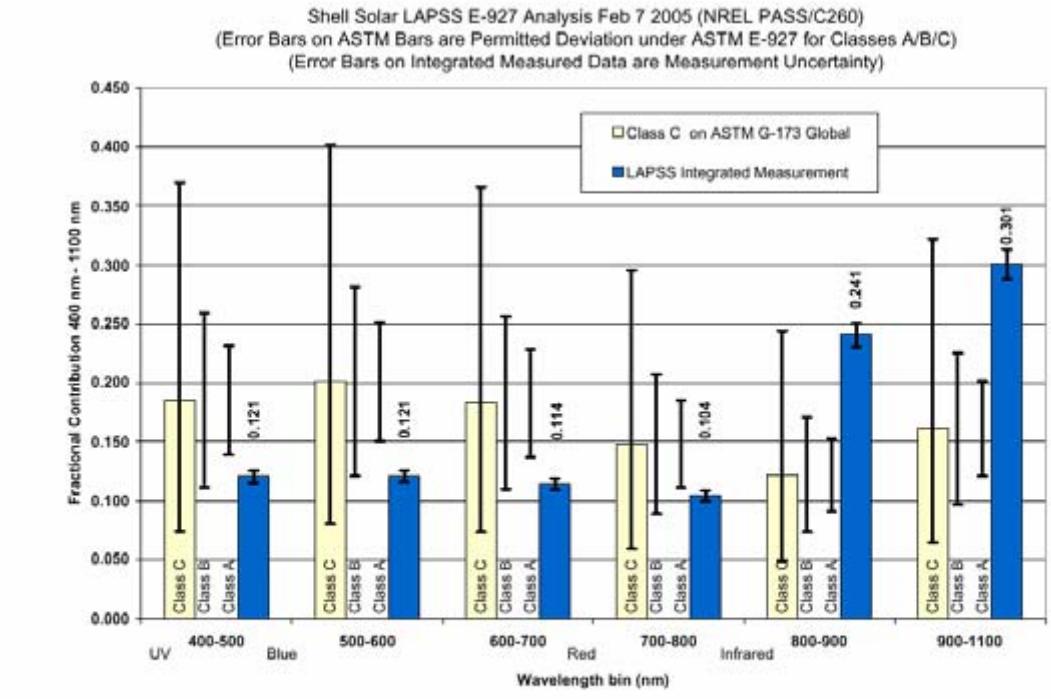

Fig. 2.15. ASTM E-927 Classification of Shell Solar LAPSS Solar Simulator based upon NREL PASS spectral data

For both the Shell Solar, and the NREL LACSS cases, it is important to note that while the classification of the simulator conveys a certain amount of information, *knowledge of the actual measured spectral distribution can be used to mathematically translate the result of measurements under each source to standard reporting conditions* [6]. It is this critical spectral data information, above and beyond the classification, that permits the transformation to Standard Reporting Conditions to be accomplished.

2.5 Updating NREL Spectroradiometer Systems

The Li-Cor, Inc., LI-1800 spectroradiometer systems have been the workhorse spectral measurement systems at NREL for over 20 years. Recently, Li-Cor announced that they would no longer manufacture the systems, as certain electronic components were no longer available. Li-Cor also felt it was not cost-effective for their small company to invest in upgrading or re-designing this instrument, so Li-Cor removed it from their product line. As this instrument is tightly integrated into the PV Measurement Group process for calibration of primary and secondary PV reference cells, it is critical that a suitable replacement for the Li-1800 systems be found before a major failure in one or any of the systems.

Several diode array spectrometer systems have been evaluated, including an Analytical Spectral Devices (ASD) Handheld, Ocean Optics Model 200 USB, and Ocean Optics Model HR 2000 High Resolution system. The ASD unit has a limitation in that it cannot be easily integrated into an automated measurement system. The supplier's software package is the only way to collect and examine data. An example of outdoor comparison between an Li-1800 spectrometer and the Ocean Optics HR 2000 is shown in Figure 2.16.

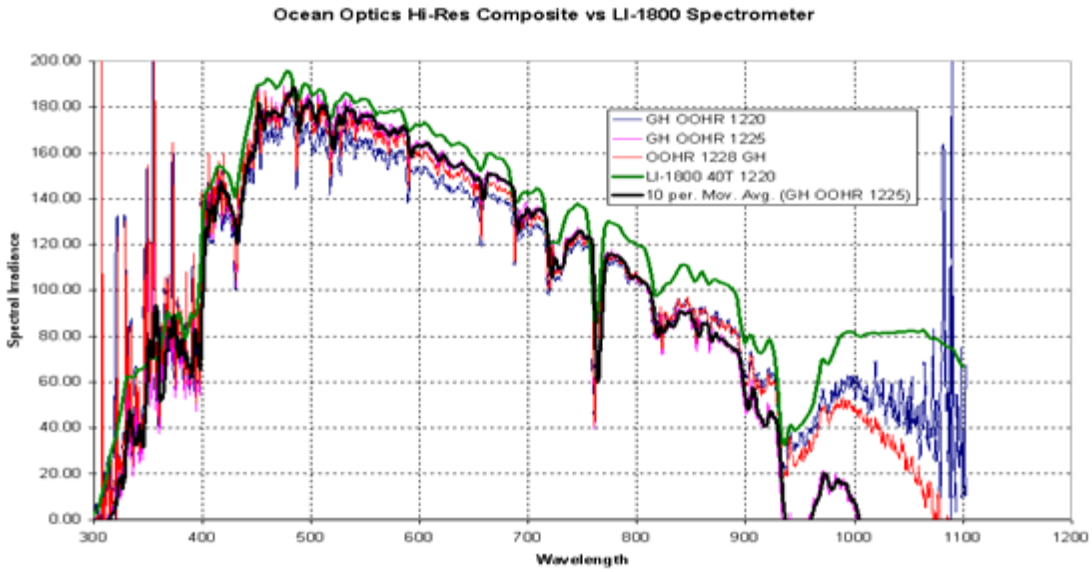

Fig. 2.16. Comparison data for LI-1800 and Ocean Optics HR 2000 Spectrometer system.

The Ocean Optics USB 200 spectrometer also relies on a specialized software package, unsuitable for integration into an automated measurement system. Finally, the Ocean

Optics HR 2000 is supplied with Dynamic Link Library (DLL) files allowing the user to integrate the system into a custom automated measurement system. However, in common with all of the diode array systems evaluated, the spectral interval of the recorded data does not match the 3.6 nm passband of the LI-1800 monochromator. This issue could be addressed mathematically with appropriate convolution integrals, but would require re-tooling of the software now used to produce NREL performance reports.

Beyond the issue of the resolution of the spectral data, diode array units without temperature control of the detector array show significant temperature drift beyond 900 nm, as shown in the test data for the Ocean Optics HR-2000 unit in Figure 2.16. The figure also shows significant noise in the wavelength region below 400 nm. Using increased data integration times could reduce this noise.

Given these limitations, further searching was done to locate systems that would have the flexibility, similar bandpass options, and better optical performance than the Li-1800 system. Extensive review of specifications and discussions with various suppliers of spectroradiometer systems lead to the selection of a classical scanning grating system candidate replacement from Instruments Systems, Inc. Model SP320 model 114. (Specifications at http://www.instrumentsystems.com/Products/spectro320.pdf) We are working with the PV Measurements and Characterization Group to obtain a demonstration unit for testing at NREL before committing to a purchase.

3.0 Broadband Calibrations and Research

Evaluating photovoltaic (PV) cells, modules, and arrays, and systems performance relies on the accurate measurement of the available solar radiation resources for conversion. Pyrheliometers (Figure 3.1) measure the shortwave (0.3 micrometer to 2.5 micrometer wavelength) solar radiation direct-beam radiation within a 5° field of view around the solar disk. Pyranometers (Figure 3.2) measure the total shortwave solar radiation, also called global or hemispherical solar radiation, in a hemispherical (2π steradian) field of view. Pyranometer measurements are used to characterize performance of flat-plate PV technologies, and pyrheliometer measurements are important for concentrating solar collector technologies.

Fig. 3.1 Pyrheliometers for measuring direct-normal solar radiation.

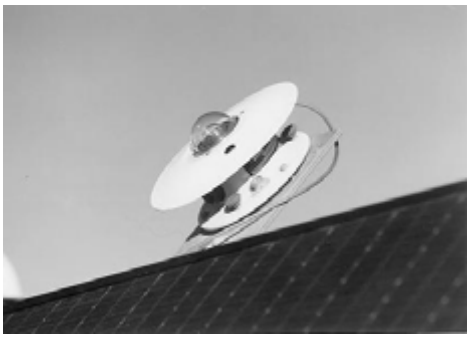

Fig. 3.2 Pyranometer for measuring global-hemispherical radiation.

The ratio between the pyranometer output signal (measured in microvolts) and the intensity of the solar power flux (measured in watts per square meter) is known as the calibration factor. NREL's Measurements and Instrumentation Team developed Broadband Outdoor Radiometer Calibration (BORCAL) procedures to characterize and calibrate pyrheliometers and pyranometers. These procedures refined and improved our Radiometric Calibration (RADCAL) techniques [7-9]. The vehicle for implementing BORCAL data collection, reporting, and data archiving is our Radiometer Calibration and Characterization (RCC) software, developed by the Measurements and Instrumentation Team (NREL, 1997).

Members of the Measurements and Instrumentation Team have worked with the U.S. Department of Energy (DOE) Atmospheric Radiation Measurement Program (ARM), National Aeronautics and Space Administration (NASA) Earth Observing System (EOS) Validation Program, World Meteorological Organization (WMO) Baseline Surface Measurement Network (BSRN), and National Oceanic and Atmospheric Administration (NOAA) Solar Radiation Research Branch (SRRB) to identify, characterize, and reduce sources of error and uncertainty in broadband shortwave radiation calibrations and measurements [10-15].

3.1 WRR Traceability: NPC 2004

The project supported the NREL Pyrheliometer Comparison (NPC) September 23 - October 3, 2003. The object of the comparison is to confirm the stability of NREL reference radiometers for broadband calibrations, and transfer WRR to participating radiometers, according to WMO protocols [10, 16]. Individual instruments are compared to a *transfer standard group* (TSG) of absolute cavity radiometers that participated directly in International Pyrheliometer Comparisons (IPC), sponsored by the World Meteorological Organization (WMO). Twenty-seven cavity radiometers participated, including instruments for the Florida Solar Energy Center (FSEC), U.S. DOE Atmospheric Radiation Monitoring program, NASA Langley Research Center, and National Oceanic and Atmospheric Administration. Pooled standard deviation of the TSG radiometers (with four from NREL) was 0.06%, confirming excellent stability of the NREL solar radiometric references, as shown in Figure 3.3. Figure 3.4 shows some of the activities that took place during the NREL Pyrheliometer Comparisons this year.

Preliminary results were deduced from the data collected over the period of the 2004 NPC and used to produce ISO-compliant calibration certificates to all participants. The writing of a final report fully documenting the NPC is in progress as of March 2005. The final version of the formal report will be posted on the Solar Radiation Research Laboratory overview website page when completed. A summary of the World Radiation Reference reduction factors derived for each participant is shown in Table 3.1.

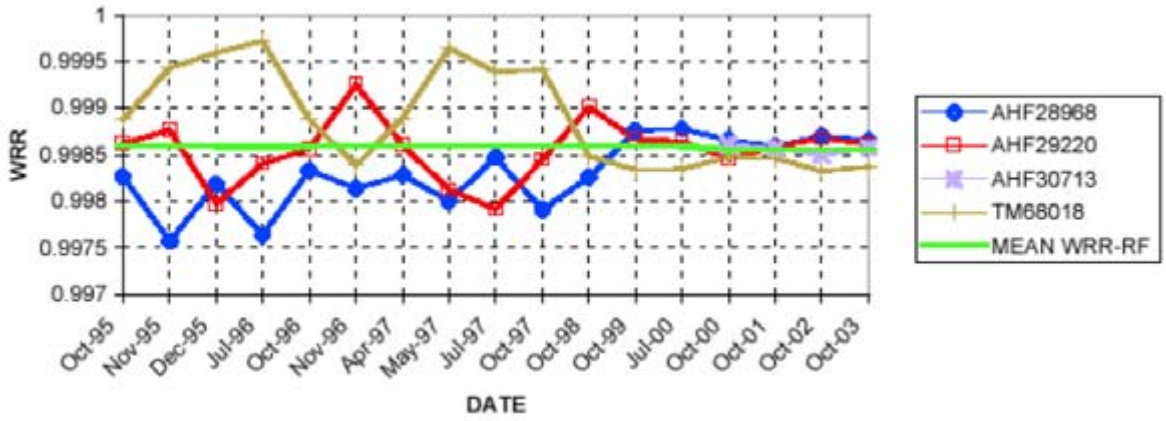

Fig.3.3. History of WRR correction factors for NREL reference.

Fig. 3.4. NREL Pyrheliometer Comparison (NPC) September 23-October 3, 2004. Top Left; NREL Metrologist I. Reda adjusts the NREL reference group of absolute cavity radiometers. Bottom left, European Solar Testing Institute (ESTI) PV Reference Cell packages tested during the comparison. Right, subset of the 17 absolute cavity radiometers participating in the NPC, including representatives from National Oceanic and Atmospheric Administration, National Aeronautics and Space Administration, Sandia National Laboratories, ESTI, and instrument manufacturer Eppley Laboratory.

In short, the standard deviations of the mean WRR reduction factors for all participants (excepting AHF30494) were less than 0.08%, and the 95% confidence interval for the uncertainty in the transfer of WRR to participants was less than or equal to ±0.35% with respect to SI units, with the exception of AHF30494 (at 0.46%).

Table 3.1. Summary Results for NPC 2004 Participating Absolute Cavity Radiometers.

Cavity Serial	WRR Transfer Factor	% Standard Deviation	Number of readings	95% confidence Uncertainty with respect to SI
AHF28968*	0.99870	0.00	1180	0.32
AHF29220*	0.99865	0.03	1180	0.32
AHF30713*	0.99856	0.04	1180	0.32
TMI68018*	0.99830	0.06	1180	0.32
AHF28553+	0.99608	0.06	518	0.35
TMI67502+	1.00048	0.08	516	0.36
AHF14915+	1.00051	0.06	236	0.34
PMO6 81109+	0.99927	0.08	288	0.36
PMO6 911204+	0.99948	0.06	291	0.34
AHF17142	0.99899	0.04	1034	0.33
AHF21182	0.99998	0.04	749	0.33
AHF23734°	0.99886	0.03	1169	0.33
AHF28964	0.99892	0.06	995	0.34
AHF29222	1.00056	0.05	761	0.34
AHF30494	0.99909	0.16	596	0.46
AHF30495	0.99791	0.05	760	0.34
AHF30170	1.00014	0.05	347	0.34
AHF31041	0.99764	0.06	800	0.34
AHF31104	0.99990	0.04	1166	0.33
AHF31105	1.00309	0.06	805	0.34
AHF31108	0.99818	0.03	1091	0.33
AHF32455	1.00087	0.07	373	0.35
ATMI68017^	1.00043	0.07	618	0.35
ATM69036^	1.00161	0.05	548	.034
AWX32448	1.00103	0.05	971	0.34
AWX32452	0.99921	0.05	1164	0.34
TMI67603	1.00173	0.04	1060	0.33
TMI68020	0.99801	0.07	1078	0.35

*** NPC 2004 NREL** Transfer Standard Reference Group Participated in WMO IPC IX.
\+ *Control instruments*, participated in WMO IPC IX in addition to TSG instruments.
° NREL NCPV National Center for Photovoltaics Reference Cavity Radiometer Test & Measurements Group

3.2 Radiometer Uncertainty Sources

Several types of detectors are used for pyrheliometer and pyranometer instruments, including silicon cells and thermal detectors such as resistance thermometers and thermopiles. We have conducted research in the first half of FY 2005 leading to a revised understanding of the sources of uncertainty in instruments based upon thermopiles, under quartz or Schott WG295 glass domes that transmit shortwave radiation from 295 nanometers (nm) to 2800 nm.

Responsivity (Rsd) of a diffuse-measuring reference pyranometer is derived in a shade-unshade calibration using Rsd = (U-S)/[B*Cos(z)], where U and S are the unshaded and shaded output voltages from the sensor, z is the zenith angle, and B is measured by an ACR (shown schematically in Figure 3.5. Procedures for this calibration are described in the American Society for Testing and Materials Standard (ASTM) E-913 [17]. NREL developed shade-unshade pyranometer calibrations using an average responsivity at 45° zenith angle for three instrument azimuth angles to integrate over geometric response variations. This procedure was modified to include a continuously shaded, or control pyranometer, and reduce the azimuth rotation angles to 60°. One may then fit responsivities to the zenith angle, Rs(z), to compute six Rs(45°). The mean of these responsivities is used for the shaded pyranometer in the component summation calibration technique [11-13].

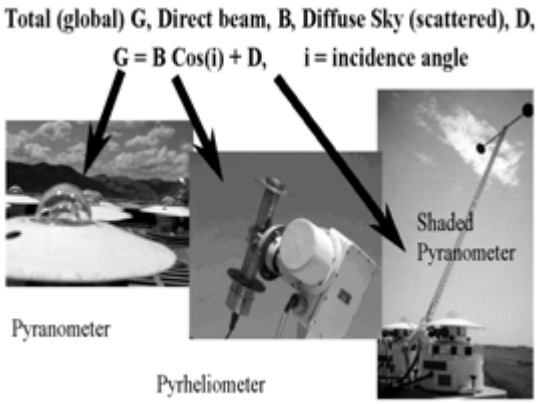

Fig. 3.5 Solar radiation measurement instruments and the components they measure.

3.2.1 Thermal Offsets

Studies of solar radiation instrumentation in climate research, as in the World Climate Change Research Program Baseline Surface Radiation Network (BSRN) participants, and others have characterized thermal "zero offsets" in thermopile pyranometers with all-black sensors measuring diffuse radiation. The offsets produce negative engineering data at night, and clear sky diffuse irradiances lower than pure Rayliegh scattering theory predicts. The offsets occur as cold junctions of the thermopile are in a different thermal environment than the absorbing junctions [15, 18-20].

Some have proposed that shade-unshade calibrations result in "cancellation" of offsets in the shaded and unshaded state [21]. We believe the offsets in the two states are different, and are a source of uncertainty in shade-unshade calibrations. It is theorized that thermal infrared exchange between the sensors, domes, and (cold) sky generate these offsets. We used the MODTRAN [22] atmospheric spectral radiative transfer code to compute shortwave and longwave (infrared, 3000 nm to 10000 nm) direct beam and sky (diffuse) radiation, as in Figure 3.6. The IR signal beyond 3000 nm is present in both the shaded

and unshaded state of a pyranometer. However, temperature of the domes and the all black absorbing sensor is significantly lower in the shaded state. Therefore, the thermal exchange between the sky and sensor/domes *cannot* be the same. For black-and-white sensors, the reference and absorbing thermopile junctions are in a similar thermal environment (see Figure 3.7). These radiometers have lower (~1 to 2 W/m^2) offsets and produce more accurate diffuse measurements.

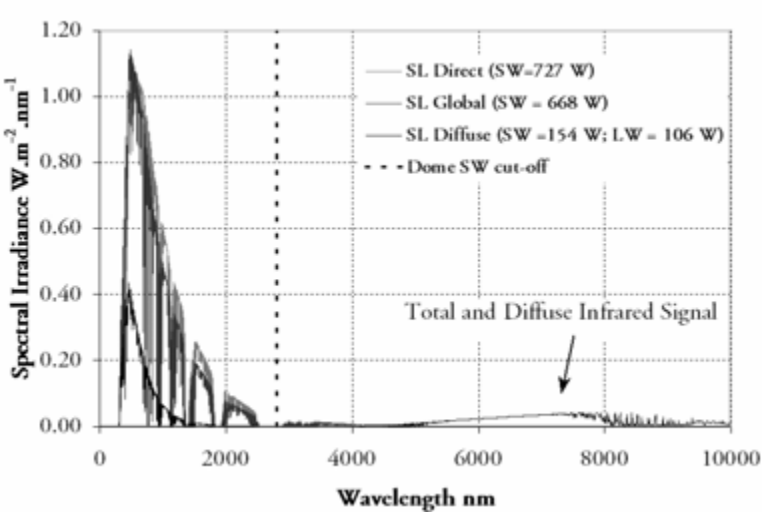

Fig. 3.6. MODTRAN 4.0 version 1.01 computed direct, hemispherical ("global") total, and diffuse sky spectra for sea level (SL). Zenith angle 45°, US Standard Atmosphere 1976, visibility 25 km. Top gray curve=direct beam, lowest curve=diffuse. Note infrared signal from 5000 nm to 10000 nm. This signal is present when the pyranometer is shaded and unshaded, however the temperature of the domes and the black sensor are significantly different.

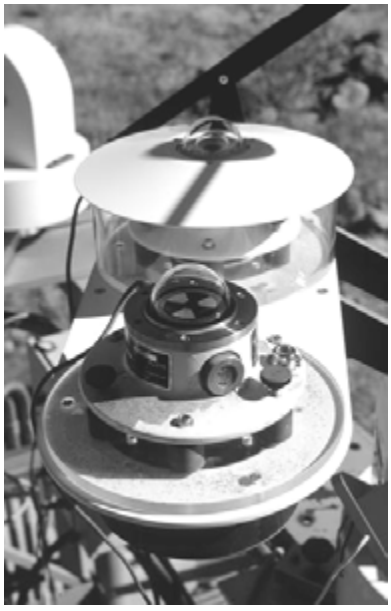

Fig. 3.7. All-black (top) and black-and-white sensor designs for thermopile pyranometers measuring diffuse sky radiation.

3.2.2 Other Spectral Errors

There is an additional spectral affect on the shade-unshade calibration in the diffuse. The diffuse sky radiation has very little energy in the shortwave region from 1000 nm to 2800 nm, while the direct beam has significant energy in that region (see Figure 3.8). Therefore, nothing affecting the direct beam total irradiance between 1000 nm and 2800 nm, such as variations in atmospheric water vapor, affects the shaded pyranometer signal. For the several different direct normal irradiances, the same shaded signal is possible from the pyranometer. MODTRAN [23] modeling of this "spectral mismatch" effect results in errors of about 0.5% in Rs, for total precipitable water vapor varying from 0.5 atm-cm to 3.5 atm-cm.

The MODTRAN spectral model was used with varying total precipitable water vapor over a reasonable range of 0.5 atm-cm to 3.5 atm-cm, to produce global total and diffuse spectra shown in Figure 3.8. The light areas between the global irradiance plots shows

the difference between the low and high water vapor conditions (dark gray=3.5 atm-cm water vapor and white=0.5 atm-cm water vapor filled curves). The changes in the diffuse spectral distribution (bottom white=3.5 atm-cm and gray=0.5 atm-cm filled curves) are minimal. For essentially the same diffuse radiation, varying water vapor content results in changes of up to 0.5% in shaded-unshade responsivities for both all-black and black-and-white detector pyranometers with respect to the global reference spectrum.

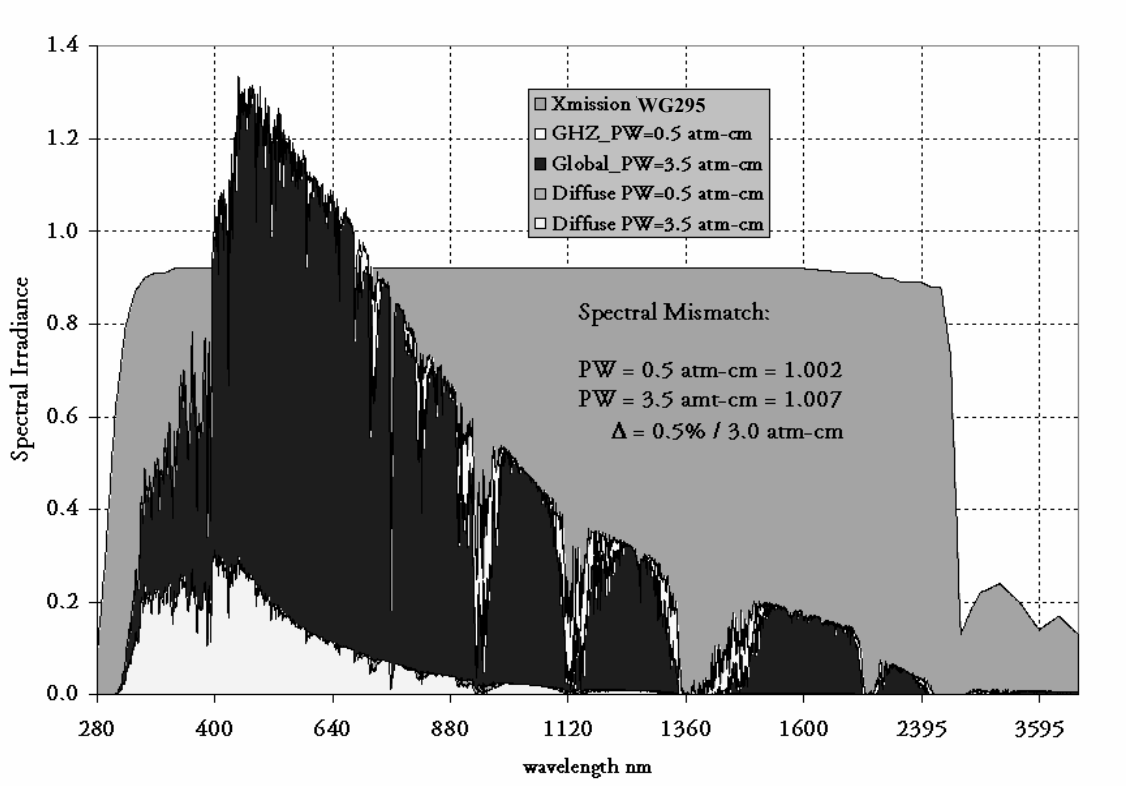

Fig. 3.8. Global (large amplitude) and Diffuse (low amplitude) horizontal spectral distributions for water vapor content of 0.5 atm-cm and 3.5 atm-cm. Gray filled area is transmission curve for quartz (WG 295) pyranometer dome material.

The "spectral mismatch" computation usually applied to evaluating photovoltaic material performance under differing spectra was used here [6]. For a given reference spectrum E_{ref} (λ), reference spectral response S_{ref}(λ), test spectrum E_{test}(λ), and device spectral response s(λ), the spectral mismatch factor resulting from the deviations of the test device response and the reference spectrum is given by:

$$M = \frac{\int E_{test}(\lambda) * s(\lambda).d\lambda \cdot \int E_{ref}(\lambda) * S_{ref}(\lambda)d\lambda}{\int E_{test}(\lambda) * S_{ref}(\lambda).d\lambda \cdot \int E_{ref}(\lambda) * s(\lambda).d\lambda} \qquad (1)$$

For the pyranometer calibrations, at each condition (high and low values of water vapor), E_{ref} is the global (unshaded) spectrum and E_{test} is the diffuse (shaded) spectrum. The reference spectral response function S_{ref}(λ), is unity, and the test spectral response

function S(λ) is the transmission curve of the glass domes. All integrals are definite with limits of integration from 285 nm to 2800 nm (the transmission band of the dome).

As indicated in Figure 3.8, the low water vapor case produces an M of 1.002; while the high water vapor case produces an M of 1.007; giving the relative difference of 100 *(1.007-1.002)/1.002 = 0.5%. If spectral conditions deviate significantly from a chosen reference spectrum (say high altitude location with respect to a sea level location), the spectral error may become site-dependant.

3.2.3 Characterizing Longwave Infrared Thermal Offset as Shortwave Error Signals

As mentioned above, experiments have been conducted that characterized thermal "zero offset" signals in thermopile pyranometers with all-black sensors. Recently, NREL used a blackbody (BB) IR source to establish a mean net IR responsivity to compute an equivalent short-wave correction voltage for the short-wave signal correction, and the associated uncertainties [14]. Figure 3.9 illustrates the BB calibration setup. Figure 3.10 shows the responses of several popular types of pyranometers to net infrared radiation measured during the laboratory calibrations.

Data were collected at BB temperatures of -35 °C, -20 °C, -10 °C, +5°C and radiometer case temperatures of -5 °C , +10°C, and 25 °C. Each BB temperature (i.e., sky) different from the plate temperature (i.e., pyranometer case) simulates atmospheric conditions that are similar to those encountered by a pyranometer outdoors. Figure 3.10 shows that the radiometer output voltage is linear with respect to the NET-IR for all pyranometers. The slope of the straight line fit is the BB responsivity of the pyranometer, RS_{bb} ,

$$Rs_{BB} = \frac{V_{TP}}{E_{bb} - E_C} = \frac{V_{TP}}{W_{NET}} \qquad (2)$$

where:

- V_{TP} is the thermopile output voltage of the pyranometer, in microvolt
- W_{NET} is the NET-IR, in W/m^2
- E_{bb} is the BB radiation, in $W/m^2 = \sigma * T^4_{bb}$, where $\sigma = 5.6697x10^{-8-8}$ $Wm^{-2}K^{-4}$, and T_{bb} is the BB temperature, in Kelvin
- E_c is the pyranometer case radiation, in $W/m^2 = \sigma * T^4_c$, where T_c is the pyranometer case temperature, in Kelvin. This temperature is measured by either a thermistor that is fitted in the pyranometer case, or a thermistor inside the aluminum mounting plate for the pyranometer.

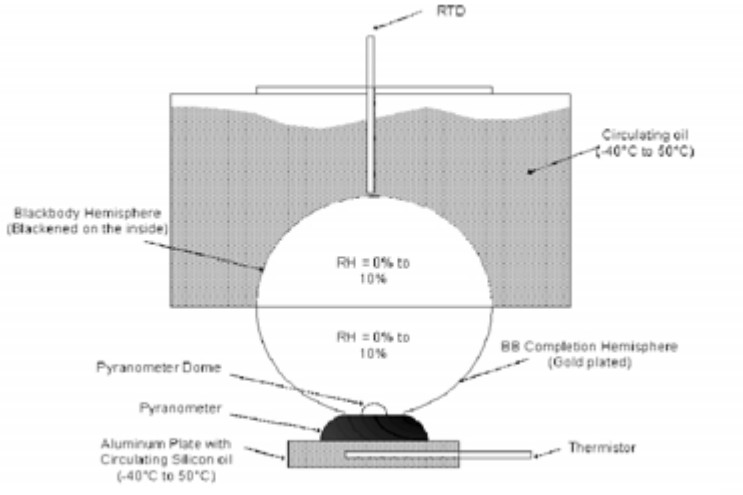

Fig. 3.9. Blackbody IR system for characterizing shortwave pyranometer net-IR response.

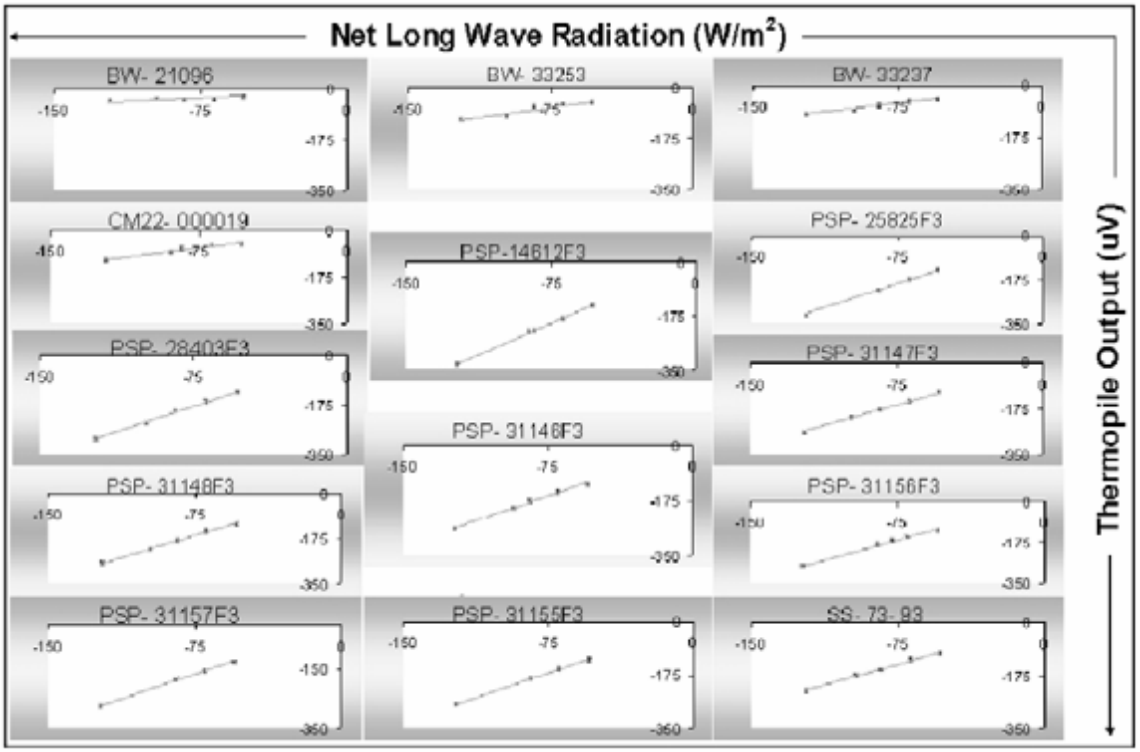

Fig. 3.10. Shortwave pyranometer signals in response to net infrared (longwave) radiation.

3.2.4 Geometric, Environmental, and Equipment Uncertainty

Additional well-known contributors to radiometer calibration and measurement uncertainty include: the accuracy of the calculation of the zenith angle; the non-Lambertian cosine response of the detector surface, temperature coefficients, linearity, thermal electromotive forces (sunshine on connectors), and electromagnetic interference (EMI). Finally, the specification and performance of the data logging equipment (resolution, precision, and accuracy) must be considered [7]. Table 3.2 lists these uncertainties.

The overall conclusion regarding this revised uncertainty analysis is that the largest sources of uncertainty are the uncertainty in the reference irradiance (cavity radiometer and diffuse pyranometer) and the thermal offsets in all-black detectors. Individual Rs computations for a point in time are accurate to 1.8%. A functional approximation to pyranometer individual response functions permitting corrections to this level of uncertainty are described in the next section. Otherwise, use of a single calibration factor for a pyranometer over all zenith angle conditions will result in data with errors up to, and even exceeding 5%.

Table 3.2 Uncertainties Individual Rs (95% confidence interval) as in Fig. 3.11.

TYPE A (Statistical)	UNC(%)	STD UNC (%)
WRR Transfer	*0.200	0.200
Cos(z) (2° Z bin)	0.010	0.005
Dif (2.5% D=>0.25% Ref.)	0.125	0.063
Temperature (2° Z bin)	0.100	0.050
Data Logger Precision	0.005	0.0025
ACR (wind, T)	0.025	0.013
Temp Chg (10° C)	0.250	0.125
Diff Offset B&W	0.125	0.063
UUT IR OFFSET	0.250	0.125
EMI/Thermal EMF	0.010	0.005

TYPE B	UNC(%)	STD UNC(%)
Logger Bias (9 uV/10 mv)	*0.090	0.090
WRR Std U95	*0.300	0.300
Cos(z) Z< 89 deg; 2° bin	0.010	0.005
Temperature (2° Z bin)	0.100	0.050
ACR Bias (M,wind, T)	0.025	0.013
Temp B (event to event) 10°C	0.250	0.125
Diff Offset B&W	0.125	0.063
UUT IR OFFSET	*0.625	0.625
Spectral error	*0.500	0.250
EMI/Thermal EMF	0.010	0.005

TOTAL	UNCERT	STD UNCERT
TYPE A	0.455	0.286
TYPE B	0.910	0.872
COMBINED	**1.017**	**0.918**

EFFECTIVE DEG. OF FREEDOM	>100
COVERAGE FACTOR (k)	2
EXPANDED UNCERTAINTY	**1.84%**

3.2.5 Responsivity Functions

Rather than evaluate offsets in the calibration (or measurement) process, a responsivity function derived from calibration data with the *offsets embedded in the result* should be used to retrieve the most accurate irradiance from a pyranometer. The far right curve in Figure 3.10b assumes e_V = data logger uncertainty (9 uV) only, and assumes the offset voltage is zero, so that value is built into the calibration result. Figure 3.11 shows the responsivity of a pyranometer versus zenith angle using NREL component summation calibration. The uncertainty in each pyranometer calibration responsivity *point* in Figure 3.11 is summarized in Table 3.2. The expanded uncertainty for each point in the curves

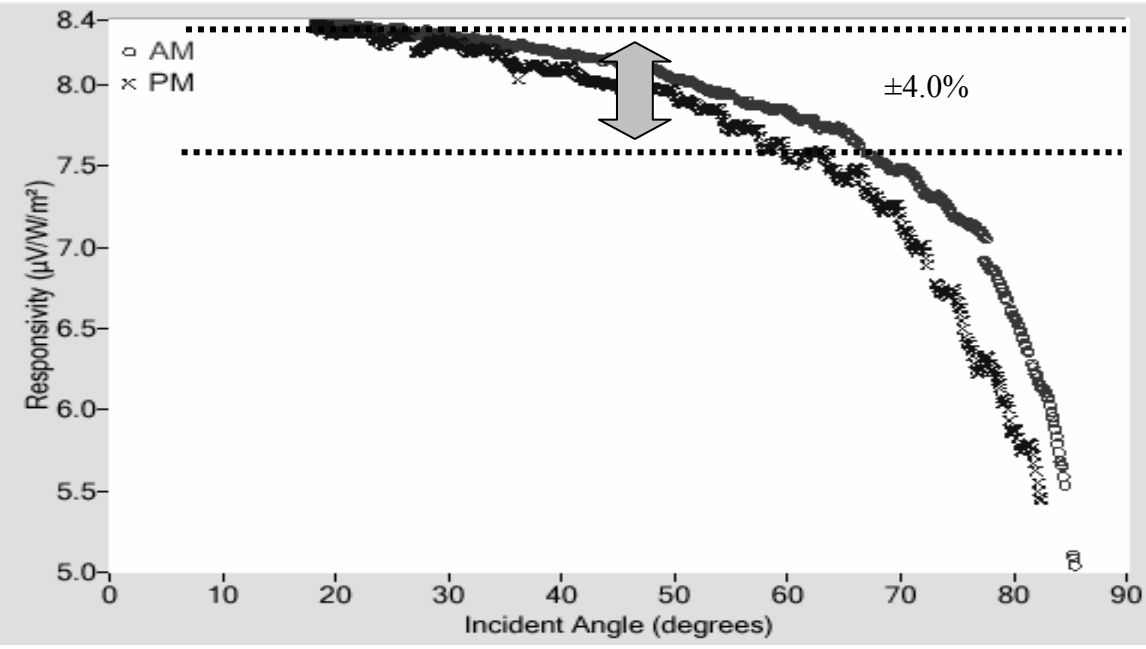

Fig. 3.11. Pyranometer responsivity versus solar zenith angle. Dotted lines are +4% and -4% away from mean Rs(45°).

of Figure 5 is about 1.8%, with coverage factor *k*=2. This is the *smallest* uncertainty that can be expected of a pyranometer, under conditions identical to the calibration conditions at a specific zenith angle. To apply corrections for a specific zenith angle, a functional approximation has been developed of the form [11, Myers, 2004 #18]:

$$Rs(z)_{AM/PM} = \sum_{i=0}^{i=46} a_i \bullet Cos^{i}(z) \qquad (3)$$

where the a_i are 46 coefficients for each morning and afternoon set of z.

With this approach, uncertainty of about ±1.8% in measured pyranometer data at any zenith angle can be achieved. Choosing any single responsivity, Rs(zo), the uncertainty in a measurement of global irradiance will change as the difference between Rs(zo) and Rs(m) changes. The uncertainty may grow to more than 10% for zenith angles sufficiently separated. When radiometers are deployed to the field, further sources of uncertainty arise, such as differing (usually lower resolution) data logging, cleanliness, and even climatological conditions, which must be considered in addition to the calibration uncertainty computed in Table 3.

3.2.6 Pyranometer Corrections from Field Data

If a measurement station is equipped to measure global total horizontal, direct beam, and accurate diffuse irradiances, one can use clear day data to perform an in-situ characterization of the responsivity variation of a pyranometer throughout the year. A recent journal article produced by NREL [24] describes the technique, summarized here.

Cloudless days are chosen to obtain data where the instruments (pyrheliometer, pyranometer, diffuse pyranometer, and where available, net infrared data (which is not essential, as shown below) were operating. The days are grouped by month and a random sample of three clear days was taken from each month. Where there were fewer than three cloudless days or data were missing, days were substituted from another year or a smaller sample for each month is used. A collection of 31 sample days composed a mock year of twelve three-day "months".

Once this information is gathered, global total pyranometer raw signals, S, are obtained by dividing irradiance by the single calibration factor used to compute the archived data. Reference global irradiances were calculated from the diffuse and direct beam instrument using the summation equation: G_r = B Cos(z) + F. "Raw" responsivities, Rs, are then computed from Rs= S/ G_r.

Plotting raw Rs versus time, significant excursions occur early and late in the day. Removing data for the pyranometer reading of less than 200 W does away with data from the very early mornings and late afternoons, where the ratio of very small numbers caused extreme values of Rs to appear. Figure 3.12 shows the resulting annual variation in Rs over a year (dark lines).

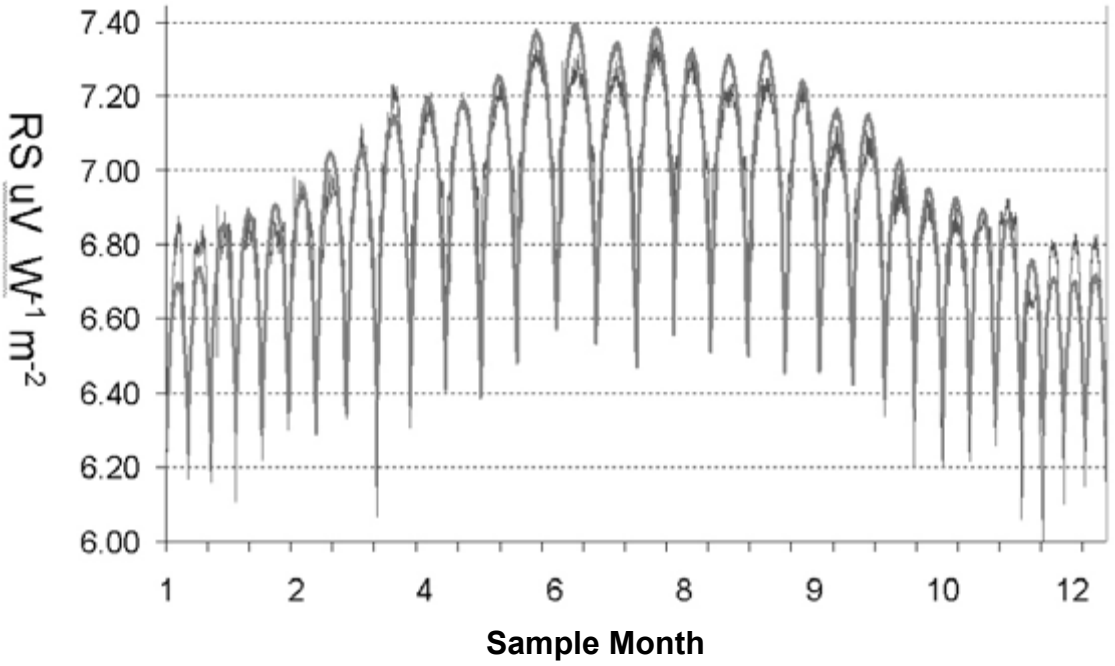

Fig 3.12. Raw Rs varies daily and yearly due to variations in zenith angle throughout the day and year respectively (dark jagged curve). Fit of Rs function of cos(Z), cos(2 πD/365) shown as smooth gray curve.

The resulting raw Rs is plotted against one of the variables, v_1. Then an appropriate regression was made, giving a function $Rs(v_1)$ relating Rs to this variable. This function was then applied to every data point, and the raw Rs was subtracted from $RS(v_1)$, yielding an absolute error value ε_1 at each v_1:

$$\varepsilon_1 = Rs(v_1) - \text{Rs}. \qquad (4)$$

The absolute error ε_1 was then plotted against the second variable v_2, a linear fit is performed, and, if the correlation was high enough, a new function $E(v_2)$ was determined by the line fit relating ε_1 to v_2. The $Rs(v_1)$ function is updated by subtracting $E(v_2)$, yielding a function for RS dependent upon v_1 and v_2:

$$Rs(v_1, v_2) = Rs(v_1) - E(v_2). \qquad (5)$$

This function is applied to each of the data points, and the absolute error from the raw Rs is compared to the next variable v_3, yielding a new $RS(v_1, v_2, v_3)$. Following this approach, an Rs function relating to any number of variables could be determined.

Independent variables used are the cosine of the zenith angle, cos(Z), the cosine of the "day angle" of the year, D_Θ = (Day number * 2*π)/365, and net-infrared, IR, measured with a pyrgeometer, if available. Note this approach treats the respective variables as truly independent variables, with no cross correlation. This assumption is not necessarily completely justified, but simplifies the method.

Next, Rs(Z, D_Θ, IR) for each data point throughout the year are computed. The smooth gray curve in Figure 3.12 shows such an Rs function. Applying the Rs functions to the millivolt signal values produces corrected irradiance values. The magnitude of the error in the correction is evaluated by comparing the new irradiance with the reference irradiance. A 95% confidence interval uncertainty can be estimated based on two times the standard deviations of the percent error distribution (assuming normality).

Example approximations found as a function of Z, D_Θ, and IR for and unventilated global PSP unit, using for the diffuse reference both a black-and-white, $Rs_{8\text{-}48}$ (Z, D_Θ IR) and an all-black detector, Rs_{PSP}(Z, D_Θ, IR), diffuse reference irradiance for instruments are shown in equations 11 and 12.

$$RS_{8\text{-}48}\ (Z, D_\Theta\ IR) = 1.5995\ (\cos(Z))\text{-}0.1003\ \cos(D_\Theta)\text{+}0.0008\ IR\text{+}7.8966 \qquad (6)$$

$$RS_{PSP}(Z, D_\Theta, IR) = 1.2083\ (\mathrm{Cos}(Z)\text{-}0.1339\ \mathrm{Cos}(D_\Theta)\text{-}0.0004\ IR\text{+}8.1952 \qquad (7)$$

Figure 3.13 is a plot of absolute error in irradiance (reference – respective irradiances, Wm^{-2}) versus the reference irradiance for the single Rs data and the $RS_{8\text{-}48}$ function corrected data. The error in original data (-30 W/m^2 to 40 W/m^2) is generally two to three times the calculated data (-10 W/m^2 to 20 W/m^2).

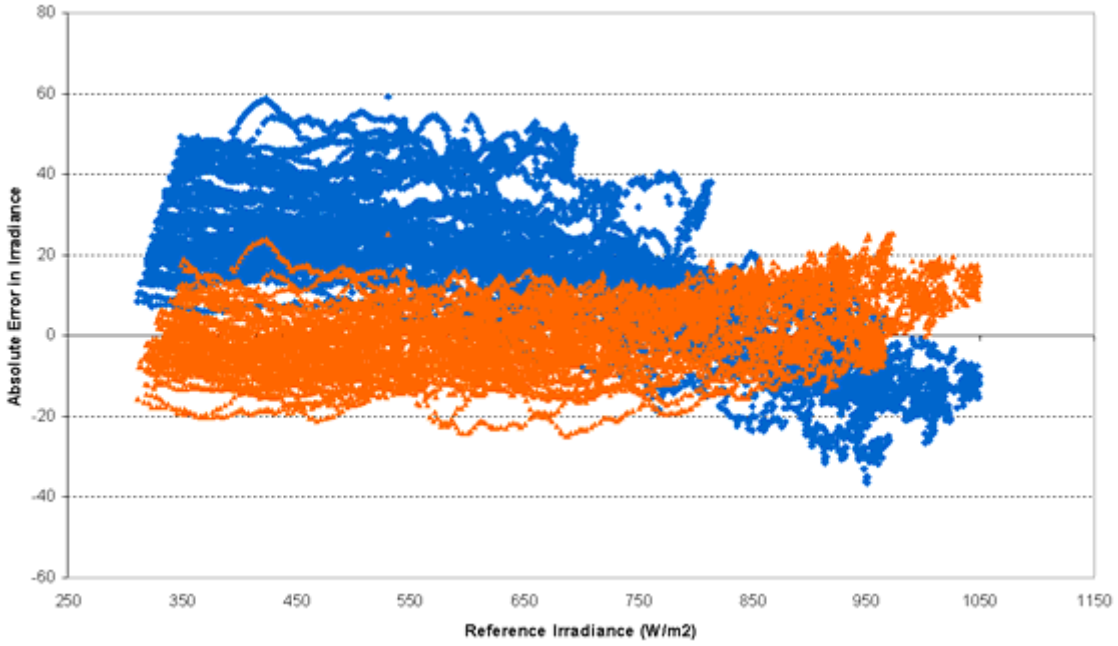

Fig. 3.13. Absolute error for single Rs (black) and $RS_{8\text{-}48}$ function corrected irradiance (gray) for all-black unventilated Precision Spectral Pyranometer.

The method was applied to pyranometers ventilated with blowers installed to keep snow, rain, and dust off the outer domes. Also, the IR thermal offset correction (using pyrgeometer measured net Infrared data) of Reda, et al., described in section 3.2.3 above, was applied to pyranometer millivolt signals. The thermal offset error voltage was

removed, resulting in corrected irradiance data. The corrected voltages were also used to produce raw responsivities (Rs*), for which functional fits Rs*(Z, D_{Θ}, IR) were produced.

As shown in Figure 3.14, the net-IR corrected data have uncertainty comparable to the Rs function corrected data. This implies that the functional approximations inherently contain a large part of the thermal offset information. The Rs*(Z, D_{Θ}) approximations produced negligible improvement over the Rs(Z, D_{Θ}) corrected data. A summary of the errors and uncertainties for each of these correction methods is summarized in Table 3.3 and Figure 3.14.

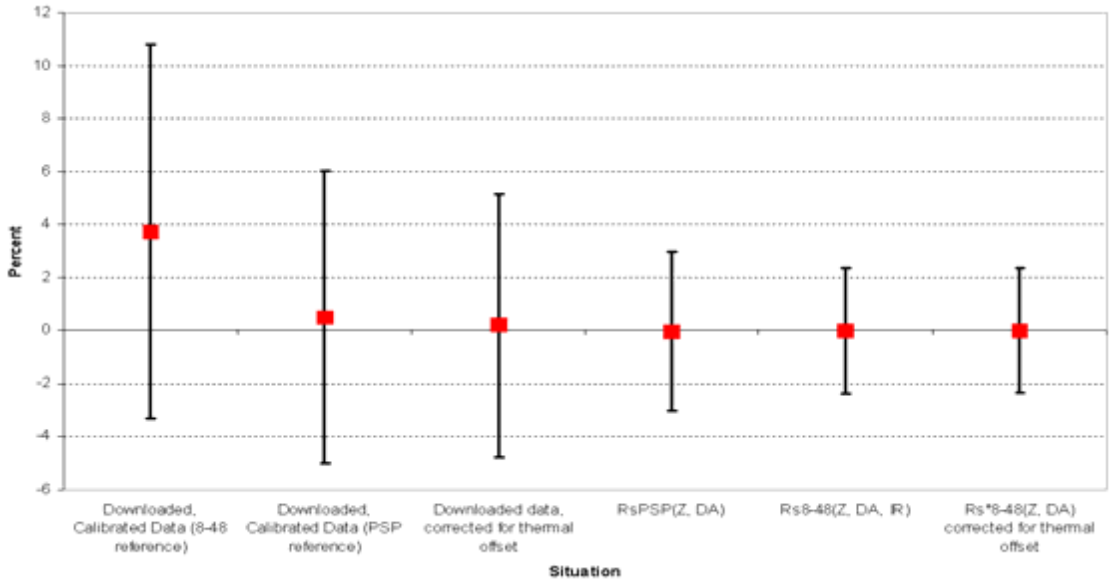

Fig. 3.14. Percent bias error (squares) and 95% confidence interval (twice standard deviation) for error distribution of uncorrected ("downloaded") and Rs function corrected global horizontal data with respect to reference global horizontal data.

The Rs function correction and constant Rs methods share certain sources of error. They use the same instruments for reference: either a diffuse PSP or 8-48, and a direct beam measuring pyrheliometer. Thermopile pyrheliometers have been shown to have a temperature dependent responsivity. The larger variation in the reference irradiance when the PSP is used for the diffuse component causes variation in RS that is difficult to reduce. The 8-48 Rs functions fit more closely and more accurate irradiance values can be computed (see Table 3.3). It appears that the thermal offset corrections are unnecessary when the function method is used. Thermal offset corrections could be applied using an estimated or average net IR value. The function method produces a dramatic decrease in global irradiance uncertainty, but it is important to note that the results of this study are instrument- and site-specific.

Table 3.3. Error and Uncertainties for calibration methods (unventilated, ventilated). Errors are with respect to computed reference irradiance.

		Irradiance Percent Error (%)		Irradiance Absolute Error (W/m^2)	
	Calibration Method	Mean	Confidence interval (uncertainty)	Mean	Confidence interval (uncertainty)
Black-and-White 8-48 Reference	Single Rs Data	3.514 **3.741**	(-3.2, 10.3) **(-3.3, 10.8)**	17.483 **16.14**	(-17.6, 52.5) **(-12.6, 44.9)**
	Single Rs Data with thermal offset corrections	1.6 **0.2**	(-4.3, 7.5) **(-4.7, 5.1)**	6.084 **4.1**	(-29.2, 41.3) **(-23.6, 31.8)**
	$Rs_{8\text{-}48}(Z, D_\Theta, IR)$	-0.103 **-0.007**	(-2.9, 2.7) **(-2.3, 2.4)**	1.246 **1.010**	(-16.6, 17.2) **(-11.4, 13.4)**
	$Rs^*_{8\text{-}48}(Z, D_\Theta, IR)$	-0.014 **0.013**	(-2.8, 2.8) **(-2.3, 2.4)**	1.032 **-1.3**	(-15.8, 17.8) **(-13.4, 10.9)**
All-Black PSP Reference	Single Rs Data	0.625 **0.5040**	(-5.2, 6.4) **(-5.0, 6.0)**	0.107 **-1.063**	(-35.7, 35.9) **(-30.2, 28.1)**
	$Rs_{PSP}(Z, D_\Theta, IR)$	-0.010 **1.018**	(-3.5, 3.5) **(-1.9, 4.0)**	**7.482**	**(-10.1, 25.0)**
	$Rs_{PSP}(Z, D_\Theta)$	-0.014 - **0.013**	(-3.5, 3.5) **(-3.0, 3.0)**	1.246 **1.482**	(-19.6, 22.0) **(-13.6, 16.6)**

3.2.7 Pyrheliometer Uncertainties

As pyrheliometer signals are compared directly with the ACR signals, there are no concerns with geometric response, or apparent thermal offsets (night-time data ~ ±1.0 W m^{-2}), so some contributions to total uncertainty listed in Table 3 disappear. However, there are new contributions to uncertainty: the pyrheliometers have windows for continuous outdoor operation, and the ACR has no window. This may lead to spectral effects similar to those seen with respect to pyranometer domes. The ACR and pyrheliometer must be pointed at the sun, so tracking errors may arise.

Figure 3.15 shows typical data for such a calibration. There are national and international standards documents that describe the procedures for calibration of field pyrheliometers from primary (absolute cavity) pyrheliometers and reference pyrheliometers [25, 26].

The shape of the response function seen in Figure 3.15 is a current topic of research. Possible explanations are the different fields of view of the reference (5.0°) and test (5.7°) pyrheliometers, environmental influences (ambient temperature, wind speed and direction), and test instrument design (thermal gradients between detector and reference thermocouples).

One on-going investigation involves looking at pyrheliometers with different configurations of shaded physical elements and recording the "dark" signals. Figure 3.16 is a photograph of a setup where one pyrheliometer has only the window/aperture shaded

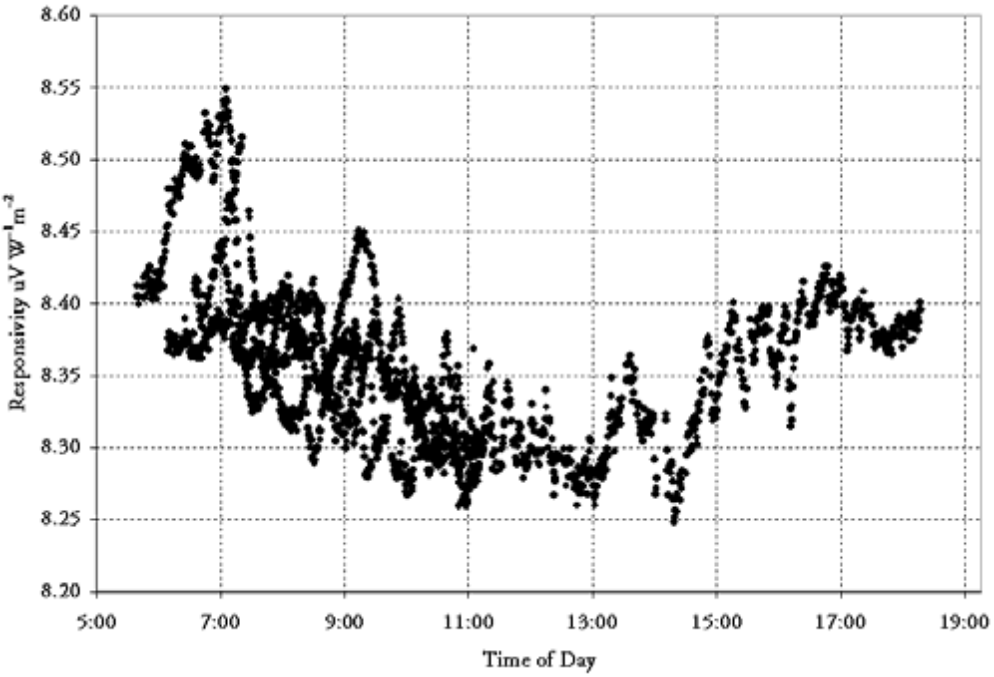

Fig. 3.15. Pyrheliometer calibration data showing the variation in responsivity (ratio of signal to reference irradiance) throughout several days. Calibration factor may be computed several ways: average of all data, or average of data over selected interval or zenith angle range.

Fig 3.16. Photo of pyrheliometers with window (lower left), window and flange (right), and flange only (top left) shaded.

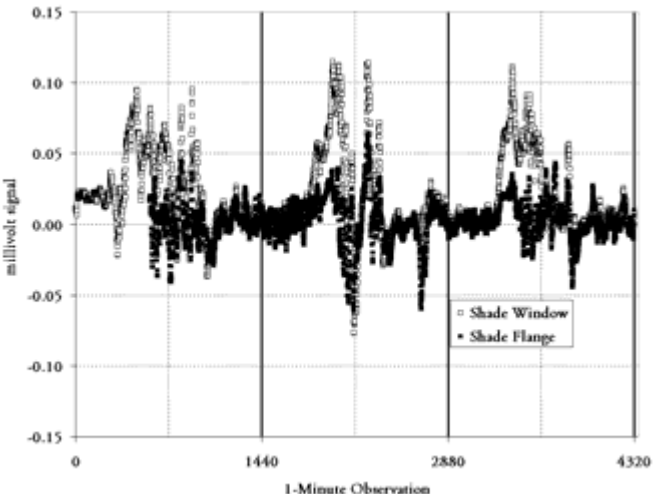

Fig. 3.17. Three days of 1 minute data for window shaded (empty square) and window and flange shaded (filled circle) "zero" data. Window-only shaded offset is larger in daytime, indicating thermal energy transfer from flange to thermocouple reference junctions.

(bottom left), another has the entire front flange of the pyrheliometer shaded (right) and a third has only the flange shaded, with an aperture to allow the direct beam to reach the

receiver (top left). The data in Figure 3.17 shows the signal from the window only and full flange shaded instruments over a three-day period. Note that the window-only shaded unit has considerably larger daytime "dark" signal than the unit with the flange fully shaded. Correlations of these offset signals with environmental data (ambient temperature, wind speed and direction, humidity, etc.) will be investigated through the rest of FY 2005.

The data in Figure 3.15 demonstrate that one must carefully document exactly how a calibration factor or responsivity for a pyrheliometer is selected or computed. An average of all the data will result in a different value of the calibration value than a selected subset of the data (restricted by zenith angle or restricted range of calibration value). The uncertainty in the calibration value, and how it was obtained, should also be documented. Radiometric calibration and measurement uncertainty is discussed in detail below.

The final tally of the pyrheliometer uncertainty components is shown in Table 3.4, with a total expanded uncertainty for each individual Rs (data point in Figure 3.12) of 1.6%.

Table 3.4. Uncertainties for individual pyrhleiometer Rs 95% confidence interval

TYPE A (Statistical)	UNC(%)	STD UNC(%)
WRR Transfer	*0.200	0.200
Temp Response UUT	0.500	0.050
Data Logger Precision	0.005	0.0025
Linearity (empirical)	0.200	0.100
ACR (wind, T)	0.025	0.013
Tracking variations	0.250	0.125
Spectral (window)	*0.500	0.500
EMI/Thermal EMF	0.010	0.005

TYPE B	UNC(%)	STD UNC(%)
Logger Bias (9 uV/10 mv)	*0.090	0.090
WRR Std U95	*0.300	0.300
Temp Response UUT	0.500	0.250
ACR Bias (M,wind, T)	0.025	0.013
Temp B (event to event) 10°	0.250	0.125
Spectral error	*0.500	0.500
Tracking Bias	0.250	0.0125
EMI/Thermal EMF	0.010	0.005

TOTAL	UNCERT(%)	STD UNCERT(%)
TYPE A	0.802	0.615
TYPE B	0.851	0.504
COMBINED	**1.169**	**0.918**

EFFECTIVE DEG. OF FREEDOM	>100
COVERAGE FACTOR (k)	2
EXPANDED UNCERTAINTY	**1.59%**

With deployment to the field, pyrheliometer data becomes subject to additional tracking and window (cleanliness) issues, differing data logger specifications, etc., requiring and additional analysis specific to the deployment to arrive at a total measurement uncertainty.

3.2.8 Revisions to ASTM Radiometer Calibration Standards

Solar Radiometry and Metrology task members participate in several consensus standards activities to support the PV industry in developing quality products with substantiated claims of performance. We provide technical expertise on radiometric measurements to ASTM committee E44 on Solar, Geothermal and Alternative Energy Sources, G03 on Reliability and Durability, and the International Lighting Commission (CIE) Technical Committee TC-72 on Solar Spectral Distributions. As a result of the above research findings, we proposed withdrawing two obsolete standards, and developed revisions to two ASTM Standards an presented them for committee review at the Jan 2005 meeting of committee G03.

The committee voted to withdraw the two obsolete standards:

E913-82(1999) *Standard Method for Calibration of Reference Pyranometers with Axis Vertical by the Shading Method*

E941-83(1999) *Standard Test Method for Calibration of Reference Pyranometers with Axis Tilted by the Shading Method*

and the two revised standards reviewed were:

G167-00 *Standard Test Method for Calibration of a Pyranometer Using a Pyrheliometer*

E816-95 *Standard Test Method for Calibration of Pyrheliometers by Comparison to Reference Pyrheliometers.*

The committee voted to submit the revised standards to ASTM ballot procedures.

This action meets the 3/31/05 milestone: "Complete proposed revised ASTM pyranometer calibration standards, reflecting state-of-the-art capabilities," for the task in the FY 2005 DRAFT AOP.

These two standards (as revised) will go forward to full ASTM committee ballot before the next meeting (June 2005). Any negative vote on the ballot actions must be addressed and deemed persuasive or non-persuasive by the committee; after which time further revisions may be made, or the approved standards proceed to full committee ballot.

The proposed modifications to the ASTM standard shade-unshade pyranometer calibration determine an average responsivity at 45° zenith angle for three instrument azimuth angles. This results in integration over geometric response variations [12]. A further modification includes a continuously shaded, or control pyranometer, and 60° rotation angles. Regression fits of responsivities to zenith angle, Rs(z) determine six values of Rs(45°), the mean of which is the calibration value for the reference diffuse (shaded pyranometer) for use in a component summation calibration.

Figure 3.18 illustrates the proposed NREL shade-unshade technique [13]. Three sequences of measurements are conducted so the data lie in the zenith angle (Z) ranges from 40° to 50°, as the final Rs will represent the Rs at Z=45°. The first shade/unshade sequence begins by shading the test and control radiometers for at least 30 time constants (150 s for an Eppley Model 8-48 pyranometer). The azimuth of the test radiometer is 0° (connector points North, to azimuth 360°). While the control pyranometer is continuously shaded, the test pyranometer is unshaded for 60 time constants (300 s for Eppley Model 8-48). The zenith angle, Z (θ =0), and signals $V_{Gt}(\theta =0)$, $V_{Dc}(\theta =0)$, and $V_B(\theta =0)$ are recorded, where

$Z(\theta =0)$ is zenith angle at azimuth $\theta = 0°$
$V_{Gt}(\theta =0)$ is signal of test unit, azimuth $\theta = 0°$
$V_{Dc}(\theta =0)$ is signal of control unit, azimuth $\theta = 0°$
$V_B(\theta =0)$ is signal of pyrheliometer, azimuth $\theta = 0°$.

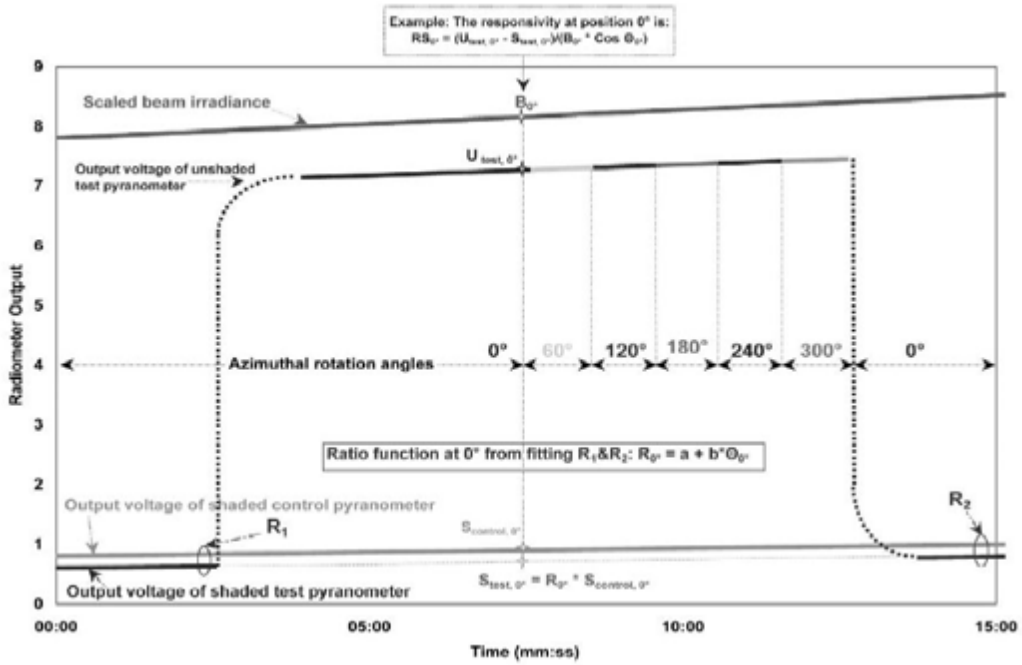

Figure 3.18. Revised shade/unshade pyranometer calibration scheme developed by NREL.

Every 60 s after the initial settling time, the unshaded test radiometer is rotated 60° in azimuth, to 60°, 120°, 180°, 240°, 300°. At each azimuth, $Z_{i,,}$ $V_{Gt}(\theta j)$, $V_{Dc}(\theta j)$, and $V_B(\theta j)$; j = 2 to 6 are recorded. The unshaded sequence ends by rotating the test radiometer back to azimuth θ =0° and shading it for 30 time constants. At the end of the 30 time constant period, the ratio of the shaded test and control radiometer signals: $k_1 = V_{Dt}(0)/V_{Dc}(0)$, where $V_{Dt}(0)$ is the signal from the shaded test unit, and the zenith angle Z_1 is recorded. The sequence ends by unshading the test units for 30 time constants.

The unshade-shade sequence above is repeated two more times. Thus three sets of shaded data, three sets of unshaded data (with rotations while unshaded), three ratios $K_i = V_{Dt}(0)i/V_{Dc}(0)_i$, and the zenith angle at which the ratios were computed, Z_i, for i = 1 to 3 are acquired. The data points (k_1, Z_1), (k_2, Z_2), (k_3, Z_3) are fit with the linear function k(Z) = a + b Z.

For each of the three sets of unshaded data, from the known zenith angles at each unshaded rotation positions, (j= 1 to 6) the shade ratio $k(Z_j)$ is calculated, and the equivalent shaded voltage is calculated from the product of the unshaded voltage and the shade ratio:

$$V_{Dt}(\eta_j) = k(Z_j) * V_{Dc}(Z_j) \qquad (8)$$

For each of the three (i= 1 to 3) unshade sequences, and j= 1 to 6 responsivities at each rotation position, the responsivity Rs[Z(i,j)] is computed:

$$R_s[Z](i,j) = \frac{[V_{Gt}(i,j) - V_{Dt}(i,j)]}{V_I(i,j)F_p \cos[Z(i,j)]} \quad \text{i=1 to 3; j= 1 to 6} \qquad (9)$$

This produces three responsivities versus zenith angle data sets for the three unshaded sequences. Linear regression is used to fit the three data points Rs(Z_i)[j] to the linear function Rs(Z)[j] = a + b Z[j] for each of the six azimuthal rotation positions (j= 1 to 6). From the six derived linear equations, the Rs at Z = 45° is computed, and the average of the six derived Rs at Z= 45° is the diffuse responsivity of the test radiometer.

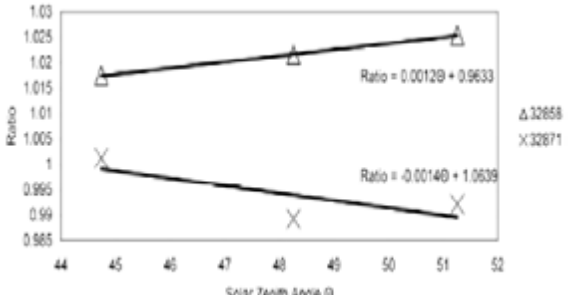

Fig. 3.19. Ratio of shaded test and control pyranometer signals with linear fits.

Figure 3.19 at left illustrates the fit of the ratio of the shaded control and two shaded test pyranometers for each of three sequences of the modified shade/unshade technique above. Figure 3.20 shows example fits of the responsivities of two test pyranometers versus zenith angle at the six different azimuth directions shown. The average of the six Rs(Z=45) derived from the fits would be the Rs applied to the test units.

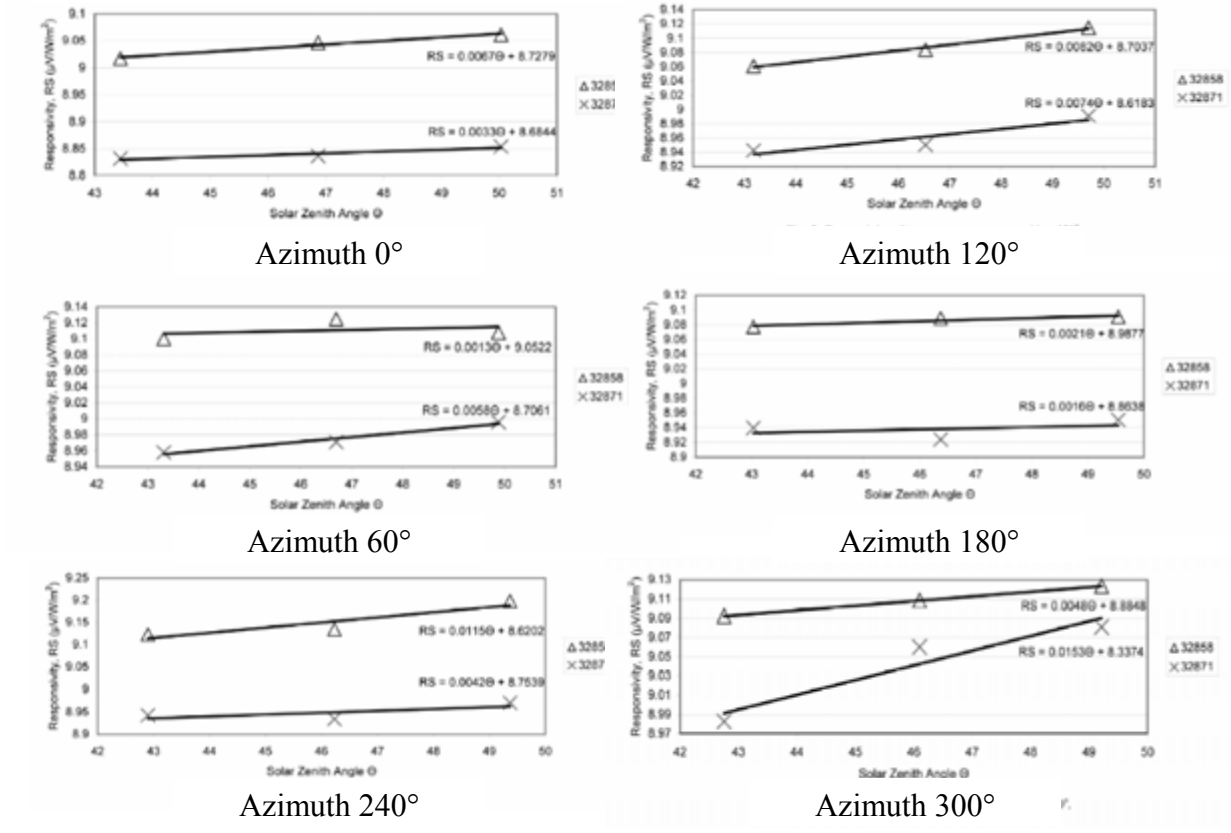

Fig 3.20. Example responsivity versus zenith angle, Rs(Z); results at six specified azimuth angles for two test pyranometers.

The average Rs(Z=45°) would be used for measuring a reference diffuse in a component summation calibration.

The Solar Radiometric and Metrology task has demonstrated that with the above modified shade-unshade technique, clear sky diffuse irradiance can be measured with an uncertainty of ± (3% of reading + 1.0 Wm^{-2}). For typical clear sky calibration conditions, the diffuse irradiance is on the order of 10% of the total global hemispherical irradiance. This means that the uncertainty in the total global reference irradiance due to uncertainty in the diffuse reference irradiance is on the order of ± (0.3% of the total reference irradiance, + 0.3 Wm^{-2}).

3.3 Upgrade of NREL Radiometer Calibration System

One source of error in Tables 3.2 and 3.4 that could be reduced is the data logger bias of 9 microvolts. This is due to the specifications of the data logger used in our Radiometer Calibration and Characterization (RCC) system for the past 5 years. In an effort to reduce this source of uncertainty, a search was undertaken to find a data logging system that would perform much better than the current system. No commercially-available system was found that met the requirements for low microvolt offsets. However, the manufacturer of a very low offset switching device used for standard voltage cell measurements offered to build a very low offset custom multiplexer to replace our older data logging system. The basis of the system is the DataProof low thermal voltage scanner shown in Figure 3.21. The company produced a custom system for our application and we purchased the system late in FY 2004.

During the first half of FY 2005, we assembled a data logging system consisting of the low offset switches, high quality off-the-shelf voltage measuring systems, and NREL designed computer controlled data acquisition. Figure 3.19 shows the assembled RCC data acquisition system configured for testing.

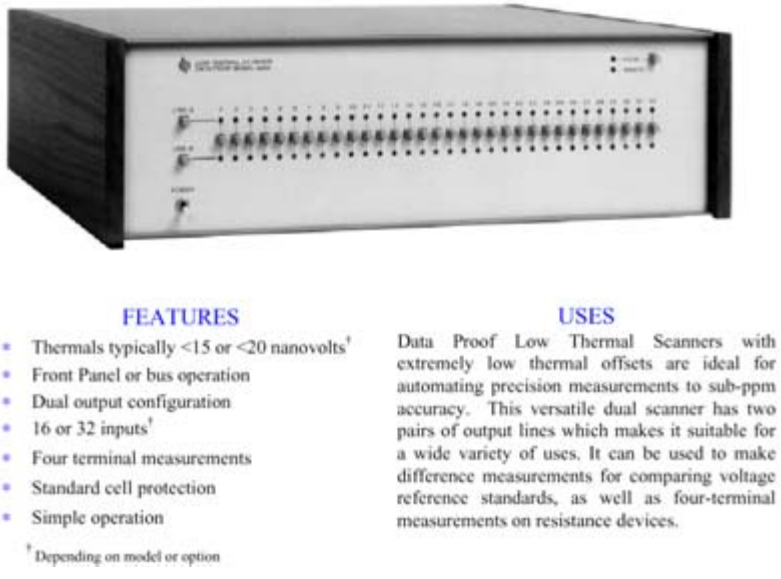

Fig. 3.21 DataProof low thermal voltage scanner, which is the basis of the new RCC data collection system. Note low voltage bias of less than 1 .0 microvolts.

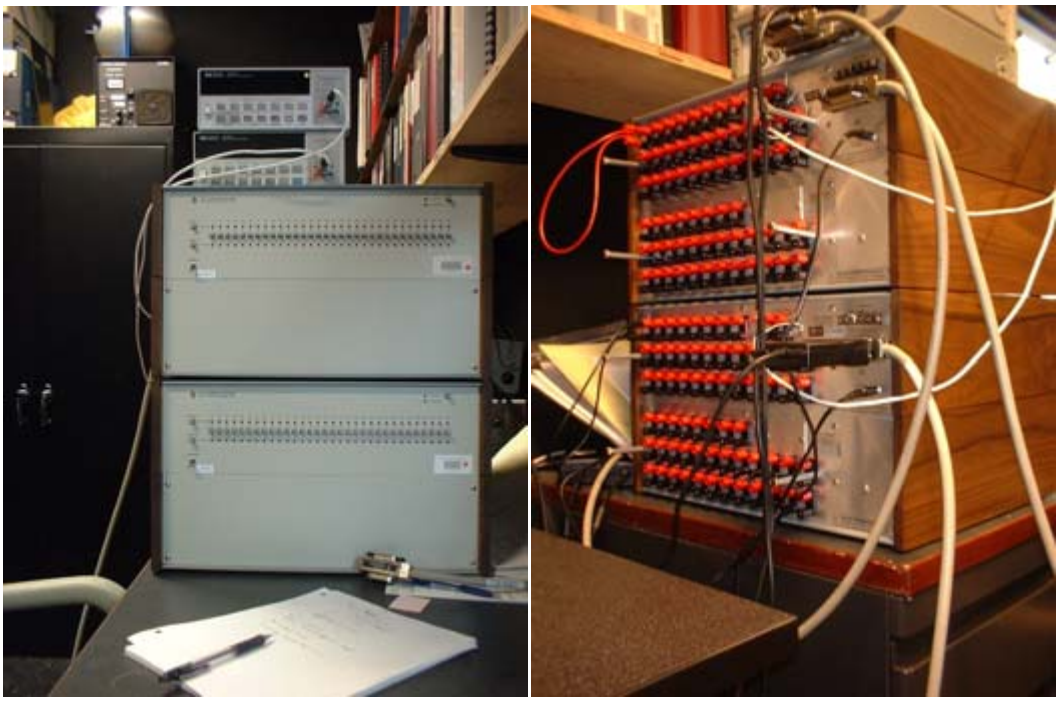

Fig, 3.22 New 100 Channel Custom NREL RCC data logger with high quality voltage measurement system configured for operational testing and control software development.

Initial tests show short circuit (zero) voltage bias errors of less than 1.0 microvolt for the new system, which is a factor of 9 improvement over the older system. Further testing is needed to evaluate and select the best configuration and software algorithms for collecting radiometer calibration data. RCC software will then be upgraded to include this data logger as a selectable instrument for collecting the calibration data. During the FY 2005 NREL Broadband Outdoor Radiometer Calibration (BORCAL) events to be conducted in the second half of FY 2005, side-by-side data collection by the new and old data loggers during an will be conducted to verify the hardware and software modifications.

4.0 Upgrades to the Measurement and Instrumentation Team Website

The Solar Radiometry and Metrology task partially supports the Solar Radiation Research Laboratory (SRRL) Measurement and Instrumentation Team (MIT) website. On April 8, 2005, the site will become one of the few examples in the world where continuous solar radiation data has been collected for 25 years. All 25 years of the collected data are available and can be downloaded from the site at http://www.nrel.gov/midc/

Figure 4.1 is the "home page" for this URL.

Fig. 4.1 Solar Radiation Research Laboratory Measurements and Instrumentation Data Center (MIDC) access home page.

Twelve measurement stations, including the SRRL Baseline Measurement System (BMS) site, are available through this page. The BMS site provides access to 138 different measurement parameters, all of interest to the solar radiation research community, are presently available from this site. Until recently, data could be downloaded forms of:

- Daily data: ASCII or compressed data selected for a single day, or period, at the data time resolution (5 minute or 1 minute data). (Example in Figure 4.2)

- Hourly monthly summary data for the MIDC Solar Radiation Monitoring stations, as shown in Figure 4.3.

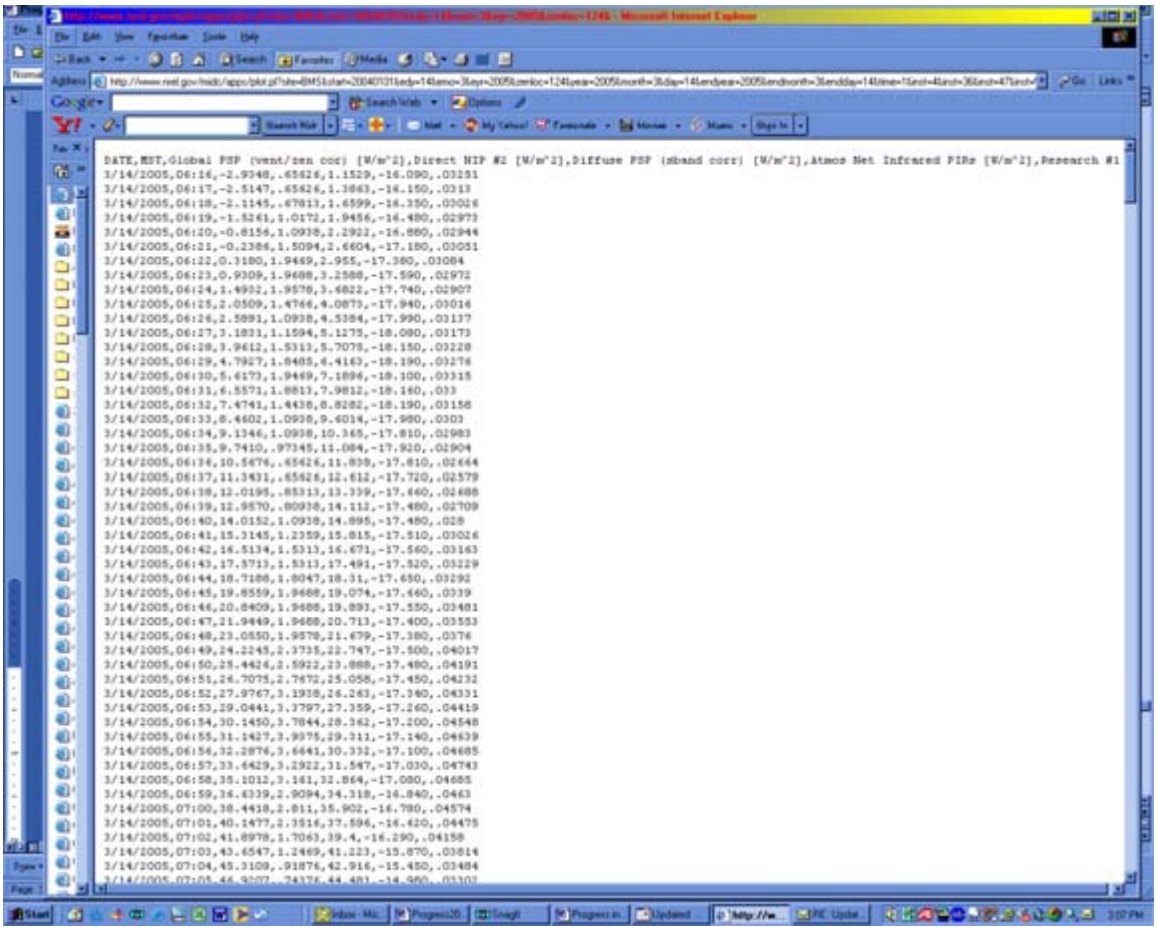

Fig. 4.2 ASCII Data download example for NREL/SRRL

The option to generate hourly data (by averaging the 1 or 5 minute raw data) is now available for any MIDC station. A new option to generate "Selected Hourly Data (ASCII)" and "Selected Hourly Data (ZIP)" is now available from the "Daily Data/Plots" page on the MIDC. The user can then select any day range and instruments. The "hourly data" was previously only available for SRRL BMS (using the QA'd monthly data from DQMS). Now it can be done for any site using the raw data, as shown in Figure 4.4.

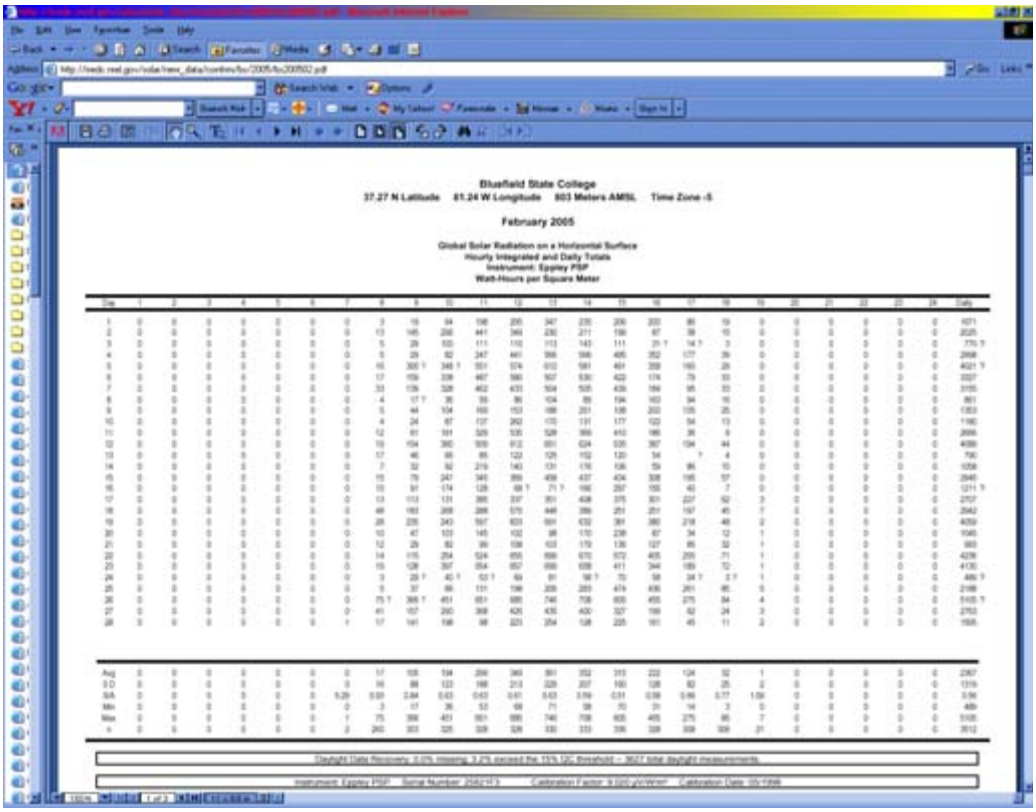

Fig. 4.3 Monthly Hourly Data Report for MIDC solar radiation monitoring station data

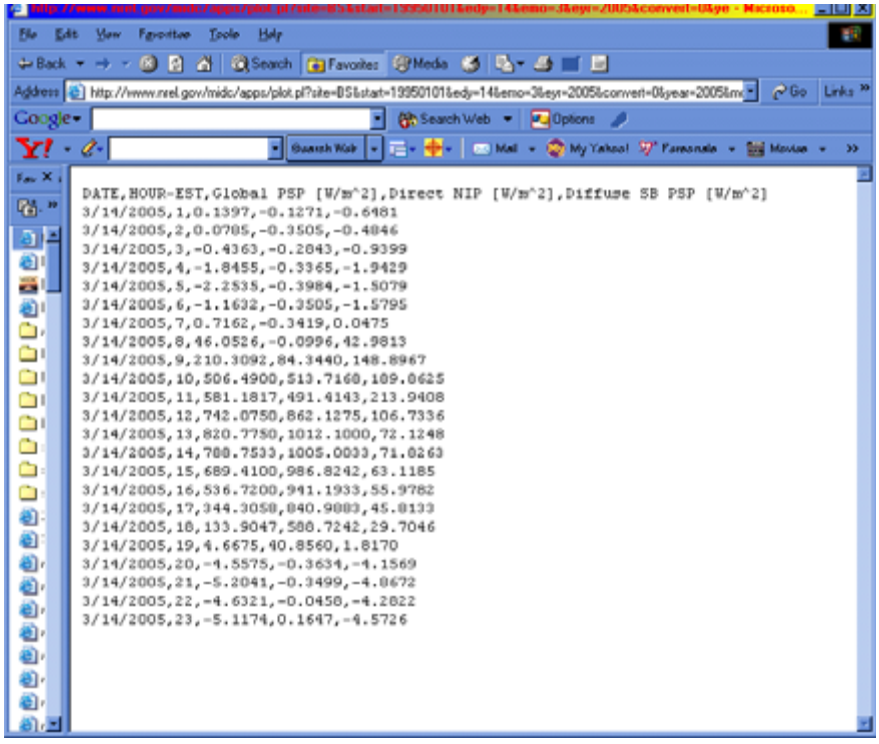

Fig. 4.4 Hourly Summary data for example solar Radiation monitoring station accessed through the MIDC website.

This capability will permit much more efficient use of the measured data for producing system performance solar radiation input file structures, verification and validation of hourly solar radiation models, data for producing Typical Meteorological Year file structures, and many other applications.

5.0 Solar Radiometric Metrology PV Industry Interactions— First Half of FY 2005

The table below is a sample of over 135 interactions documented with the PV industry, academia, and other national and international laboratories over the first half of FY 2005.

Table 5.1 Industrial Academic, National an International Laboratory interactions

Contact	Topic	Outcome
GE Global Research Niskayuna, NY Oct 18	Broadband and Spectral Models developed at NREL and Applications to PV system design, testing and performance	GE R&D requested numerous NREL and Journal publications and references. Established communication between NREL experts and GE research participants.
SmartSolar Inc, Rochester NY Oct 20	NREL capabilities for outdoor testing and performance reporting on modules	Referred to NREL Outdoor test facility operations for discussions
Ultradots Fremont, CA Oct 20	Spectral distribution of xenon arc solar simulators	Provided sample spectral distributions for theoretical calculations
Oklahoma University Oct 28	Selection of reference pyranometer for indoor calibration system, comparison of calibration techniques	Provided references and publications on pyranometer calibration issues
NASA CERES Instrument Working Group Analytical Services and Materials Nov 9	Inquires on pyranometer thermal offset data for correcting ground truth measurements for satellite data validation	Provided sample data, references and publications RE: radiometer characteristics.
Natural Resources Canada CANMET Energy Technology Centre Nov 17	Influence of thermopile dark offsets on pyranometer calibration techniques using indoor integrating sphere versus outdoor results.	Shared data results and example calibration reports.
Sandia National Laboratories Albuquerque NM Nov 17	Solar "fuel" resource components to System Driven Approach for PV R&D and system evaluation	Supplied examples of types of data required and ability to correctly statistically modulate data to simulate real environment.
Energy Plus Hemet Ca Nov 17	Request for PV Panel outdoor testing capabilities.	Referred to Outdoor Test Facility operations.
Sandia National Laboratory Nov 30	Basic pyranometer performance data.	Supplied references, publications, calibration results for radiometers.
PV Measurements, Boulder CO Dec 06	Spectroradiometer and solar simulator calibrations traceable to NIST references for PV test equipment.	Verified accuracy and uncertainty in PV testing equipment for research and commercial community

Contact	Topic	Outcome
General Motors R& D Center Warren, MI Dec 08	"one sun" Calibration of Pyranometers	Will include radiometers in next NREL BORCAL event to provide characterized radiometer responses.
Regional Development Corp. Santa Fe NM Dec 21	Requested data to assess ranking of solar resources by region	referred to NREL Renewable Resources Data Center (RREDC) and suggested various statistical algorithms for ranking sites.
Sunpower Geo Sunnyvale, CA Jan 06	Module Energy Rating Standards and Data	NREL reference reports and draft standards shared.
University of Michigan School of Natural Resources Ann Arbor,MI Jan 07	Solar Position Algorithm calculations	Shared code and web accessible test site.
University of Maine Resource Economics and Policy Orono, ME Jan 13	Photosynthetically Active Radiation (PAR) model for crop applications	Suggestions on using Bird clear sky model and PAR conversion routine
Tuross Corp Portola CA Jan 19	Cavity radiometer information	Referred to inventor and manufacturer of instrument in question.
Arizona Public Service Phoenix, AZ Jan 19	Direct Normal Irradiance for Korea	Put in contact with Korean Energy Research Institute (KEIR) data collection colleagues and NASA Surface Solar Energy Website.
National Institute of Standards and Technology Gaithersburg MD Jan 21	Pyranometer Thermal Offset data and corrections.	Shared experimental data, draft publications, and references.
Deutsche Luft und Raumfahrt Institute (DLR) Jan 26	SMARTS spectral model applications and references	Provided model and troubleshooting of user interface.
Swiss Federal Institute for Technology (EPFL) Lausanne Switzerland Feb 9	SMARTS spectral model	Hints for using for high altitude long duration solar powered manned aircraft design
Florida Solar Energy Center Cocoa, FL Feb 24	Pyranometer calibration issues	Shared example calibration results, consensus on data processing techniques and sources of differences
Shell Solar Camarillo, CA (Feb 05)	Pulse spectral simulator measurements	Data provided to improve accuracy in PV product testing,
Florida Solar Energy Center Cocoa FL Mar1	Request to measure spectral distribution of re-lamped FSEC Spire 660 Solar Simulator	ISO 17025 compliant calibration PV module certification

6.0 Major Publications

Lester, A., D. R. Myers, A Method for Improving Global Pyranometer Measurements by Modeling Responsivity Functions. *Solar Energy*, 2005. **In Press**

Reda, I., J. Hickey, C. Long, D. Myers, T. Stoffel, S. Wilcox, J.J. Michalsky, E.G. Dutton, D. Nelson, Using a Blackbody to Calculate Net-Longwave Responsivity of Shortwave Solar Pyranometers to Correct for Their Thermal Offset Error During Outdoor Calibration Using the Component Sum Method. *Journal of Atmospheric and Oceanic Technology*, 2005. **In Press**.

ASTM Standards G167-00 *Standard Test Method for Calibration of a Pyranometer Using a Pyrheliometer (REVISION)*

ASTM Standard E816-95 *Standard Test Method for Calibration of Pyrheliometers by Comparison to Reference (REVISION)*

Book Chapter for "Recent Progress in Solar Energy" Nova Science Publishers, Inc. 400 Oser Avenue, Suite 1600 Hauppauge, NY 11788 :

Myers, D., I. Reda, and S. Wilcox, "Solar Radiation Measurements, Instrumentation, and Uncertainty "

7.0 Conclusion

A great deal of progress in understanding the sources of uncertainty in broadband radiometer measurements has been accomplished in the period covered by this report. The Solar Radiometric Metrology task has maintained ISO 17025 compliant traceability for solar and optical radiation calibrations and measurements. This includes monitoring the stability of the World Radiation Reference scale for NREL reference cavity radiometers and maintaining the National Institute of Standards and Technology Scale of Spectral Irradiance. We revisited and revised our analysis of uncertainty for both broadband and spectral measurement systems. We measured and characterized the performance of several NREL research and PV industry solar simulators, providing data essential for translating PV performance measurements to Standard Reporting Conditions. Our research has led to new insights into sources of error in broadband radiometers, and improved methods of correcting for environmental influences on broadband measurement data. Revisions to existing (ASTM) standard procedures for radiometer calibrations have been developed and put before the consensus standards community for approval later in FY 2005. We are upgrading the radiometer calibration data acquisition system to remove a known bias error from our Broadband Outdoor Radiometer Calibrations and Radiometer Calibration and Characterization system, and have identified a replacement for obsolescent and aging workhorse spectroradiometers essential to primary and secondary PV reference call calibrations. We have documented over 135 separate interactions with the PV industry, academia, other national

laboratories, and PV system designers on a wide range of topics, including instrumentation, calibrations, broadband and spectral modeling, solar radiation resource data, module and systems energy ratings, and indoor and outdoor PV testing methods. Much of the above have been documented a series of journal articles and conference papers, disseminating our research results to both the scientific and industrial community.

8.0 References

[1] ASTM, Standard Test Methods for Electrical Performance of Nonconcentrator Terrestrial Photovoltaic Modules and Arrays Using Reference Cells, Standard E1036. 1998 American Society for Testing and Materials, West Conshohocken, PA.

[2] Walker, J. H., et al., NBS Special Publication 250-20 "Spectral Irradiance Calibrations". 1987 National Institute of Standards and Technology

[3] BIPM, Guide to the Expression of Uncertainty in Measurement. Published by ISO TAG 4, 1993 (corrected and reprinted, 1995) in the name of the BIPM. ISBN 92-67-10188-9, 1995. 1995 BIPM, IEC, IFCC, ISO, IUPAC, IUPAP and OIML. 1995

[4] Taylor, B. N., C E Kuyatt, Guidelines for Evaluation and Expressing the Uncertainty of NIST Measurement Results. NIST Technical Note 1297 1993 National Institute of Standards and Technology

[5] ASTM, Standard Specification for Solar Simulation for terrestrial Photovoltaic Testing ASTM Standard E-927. 1997 American Society for Testing and Materials, West Conshohocken, PA.

[6] ASTM, Standard Test Method for Determination of the Spectral Mismatch Parameter Between a Photovoltaic Device and a Photovoltaic Reference Cell ASTM Standard E973M-96 American Society for Testing and Materials, West Conshohocken PA. 1996

[7] Myers, D. R., T L Stoffel, S Wilcox, I Reda, A Andreas, Recent Progress in Reducing the Uncertainty in and Improving Pyranometer Calibrations. *ASME Journal of Solar Energy Engineering*, 2002. 124: p. 44-50.

[8] Myers, D. R., I. Reda, S. Wilcox, A. Andreas,. Optical Radiation Measurements for Photovoltaic Applications:
Instrumentation Uncertainty and Performance. in 50th Annual Conference of the Society of Photo-optical Instrumentation Engineers, Organic Photovoltaics V. 2004. Denver, CO: SPIE Bellingham, Washington.

[9] Myers, D. R.K. A. Emery T. L. Stoffel, Uncertainty Estimates of Global Solar Irradiance Measurements Used to Evaluate PV Device Performance. *Solar Cells*, 1989. 27: p. 455-464.

[10] Reda, I., T Stoffel, D Myers, Calibration of a Solar Absolute Cavity Radiometer with Traceability to the World Radiometric Reference. NREL/TP-463-20619 1996 National Renewable Energy Laboratory see http://www.nrel.gov/docs/legosti/fy96/20619.pdf

[11] Reda, I., Improving the Accuracy of Using Pyranometers to Measure Clear Sky Global Irradiance NREL/TP-560-24833. NREL/TP-560-24833 1998 National Renewable Energy Laboratory

[12] Reda, I., D Myers, Calculating the Diffuse Responsivity of Solar Pyranometers. NREL/TP-560-26483 1999 National Renewable Energy Laboratory

[13] Reda, I., T. Stoffel, D. Myers, A Method to Calibrate a Solar Pyranometer for Measuring Reference Diffuse Irradiance. Solar Energy, 2003. 74: p. p. 103-112.

[14] Reda, I., J. Hickey, C. Long, D. Myers, T. Stoffel, S. Wilcox, J.J. Michalsky, E.G. Dutton, D. Nelson, Using a Blackbody to Calculate Net-Longwave Responsivity of Shortwave Solar Pyranometers to Correct for Their Thermal Offset Error During Outdoor Calibration Using the Component Sum Method. *Journal of Atmospheric and Oceanic Technology*, 2005. In Press 2005.
[15] Dutton, E. G., J. J. Michalsky, T. Stoffel, B. W. Forgan, J. Hickey, T. L. Alberta, I. Reda, Measurement of Broadband Diffuse Solar Irradiance Using Current Commercial Instrumentation with a Correction for Thermal Offset Errors. *Journal of Atmospheric and Oceanic Technology*, 2001. 18(3): p. 297-314.
[16] WMO, OMM No. 8 Guide to Meteorological Instruments and Methods of Observation.5th ed. Vol. 8. 1983, Geneva, Switzerland: Secretariat of the World Meteorological Organization.
[17] ASTM, Standard Test Method for Calibration of a Pyranometer Using a Pyrheliometer ASTM G167-0. ASTM G167-00 2000 American Society for Testing and Materials
[18] Gulbrandsen, A., On the Use of Pyranometers in the Study of Spectral Solar Radiation and Atmospheric Aerosols. *Journal of Applied Meteorology*, 1978. 17: p. 899-904.
[19] Haeffelin, M., A.M. Smith, J.R. Mahan,C.K. Rutledge, S. Kato. Surface Shortwave Radiation Measurements: Experimental Tests and Numerical Simulations of Pyranometers. in Ninth ARM Science Team Meeting. 1999. San Antonio, TX: U.S. Dept. of Energy.
[20] Haeffelin, M., S. Kato, A.M. Smith, C.K. Rutledge,T.P. Charlock, J.R. Mahan,, Determination of the Thermal Offset of the Eppley Precision Spectral Pyranometer. *Applied Optics*, 2001. 40(4): p. 472-484.
[21] Philipona, R., Underestimation of solar global and diffuse radiation measured at the Earth's surface. *Journal of Geophysical Research*, 2002. 107(D22): p. ACL 15-1-ACL 15.8.
[22] Anderson, G. P., A. Berk, P. K. Acharya, M. W. Matthew, L. S. Bernstein, J. H. Chetwynd, Jr., H. Dothe, S. M. Adler-Golden, A. J. Ratkowski, G. W. Felde, J. A. Gardner, M. L. Hoke, S. C. Richtsmeier, B. Pukall, J. B. Mello, and L. S. Jeong. MODTRAN4: radiative transfer modeling for remote sensing. in Optics in Atmospheric Propagation and Adaptive Systems III;. 1999: Society of Photo-Optical Instrumentation Engineers Bellingham, WA.
[23] Berk, A., et al. MODTRAN4 Radiative Transfer Modeling for Atmospheric Correction. in SPIE Proceedings, Optical Spectroscopic Techniques and Instrumentation for Atmospheric and Space Research III Vol 3756. 1999: Society for Photo-Optical Instrumentation Engineers.
[24] Lester, A., D. R. Myers, A Method for Improving Global Pyranometer Measurements by Modeling Responsivity Functions. *Solar Energy*, 2005. In Press.
[25] ISO, Standard 9050: Solar Energy--Calibration of Field Pyrheliometers by Comparison to a Reference Pyrheliometer. 1990 American National Standards Institute, New York NY
[26] ASTM, Standard Test Method for Calibration of a Pyrheliometers by Comparison to Reference Pyrheliometers ASTM E 816-95. ASTM G167-00 2000 American Society for Testing and Materials

REPORT DOCUMENTATION PAGE

Form Approved
OMB No. 0704-0188

PLEASE DO NOT RETURN YOUR FORM TO THE ABOVE ORGANIZATION.

1. REPORT DATE *(DD-MM-YYYY)*	2. REPORT TYPE	3. DATES COVERED *(From - To)*
September 2005	Technical Report	

4. TITLE AND SUBTITLE
FY 2005 Midyear Progress Report on Solar Radiometry and Metrology Task PVC57301: October 1, 2004 to March 15, 2005

5a. CONTRACT NUMBER
DE-AC36-99-GO10337

5b. GRANT NUMBER

5c. PROGRAM ELEMENT NUMBER

6. AUTHOR(S)
D.R. Myers, T.L. Stoffel, A.A. Andreas, S.M. Wilcox, I. Reda, M. Anderberg, P. Gotseff, B. Kay

5d. PROJECT NUMBER
NREL/TP-560-37954

5e. TASK NUMBER
PVC57301

5f. WORK UNIT NUMBER

7. PERFORMING ORGANIZATION NAME(S) AND ADDRESS(ES)
National Renewable Energy Laboratory
1617 Cole Blvd.
Golden, CO 80401-3393

8. PERFORMING ORGANIZATION REPORT NUMBER
NREL/TP-560-37954

9. SPONSORING/MONITORING AGENCY NAME(S) AND ADDRESS(ES)

10. SPONSOR/MONITOR'S ACRONYM(S)
NREL

11. SPONSORING/MONITORING AGENCY REPORT NUMBER

12. DISTRIBUTION AVAILABILITY STATEMENT
National Technical Information Service
U.S. Department of Commerce
5285 Port Royal Road
Springfield, VA 22161

13. SUPPLEMENTARY NOTES

14. ABSTRACT *(Maximum 200 Words)*
This report documents technical details for work performed in the Solar Radiometry and Metrology Task PVC57301 in the period from October 1 2004 to March 15 2005.

15. SUBJECT TERMS
radiometry; metrology; broadband; spectral; calibrations

16. SECURITY CLASSIFICATION OF:			17. LIMITATION OF ABSTRACT	18. NUMBER OF PAGES	19a. NAME OF RESPONSIBLE PERSON
a. REPORT	b. ABSTRACT	c. THIS PAGE			19b. TELEPHONE NUMBER (*Include area code*)
Unclassified	Unclassified	Unclassified	UL		

Standard Form 298 (Rev. 8/98)
Prescribed by ANSI Std. Z39.18